Functionality properties of complexes of sulfophthalocyanine with semiconductor nanocrystals

School of Electrical Engineering

Thesis submitted for examination for the degree of Master of Science in Technology.

Espoo 03.08.2016

Thesis supervisor:
Professor Ilkka Tittonen

Aalto University
School of Electrical Engineering

ABSTRACT OF
MASTER'S THESIS

Author: Daler Dadadzhanov

Title:
Functionality properties of complexes of sulfophthalocyanine with semiconductor nanocrystals

Date: 03.08.2016	**Language**: English	**Pages**: 70

Department of Micro- and Nanosciences

Professorship: S-129 Physics of Micro and Quantum Systems

Supervisor: Professor Ilkka Tittonen
Advisor: Dr. Anna Orlova

Currently, research in the biomedical field is one of the most promising and strategically important. Special attention is paid to the use of nanostructured materials as biosensors and new generation drugs. Nanostructures offer great promise in cancer targeting applications due to their unique optical properties. A shining examples of nanostructured materials are semiconductor nanocrystals: quantum dots and quantum rods. Colloidal semiconductor quantum nanocrystals are single crystals of a few nanometers in size (typically about 2-10 nm).

In this work an investigation of conditions of phthalocyanine aggregation in complexes with NC's in aqueous media and dimethyl sulfoxide (DMSO) was performed, in particular, investigation of the effect of the size and shape of the nanocrystals on the phthalocyanine aggregation in complexes.

Complexes of CdSe/ZnS nanocrystals with phthalocyanine molecules have been formed via the electrostatic interaction between nanocrystals solubilizer molecules and phthalocyanine. It has been found that, the formation of nanocrystals/ phthalocyanine complexes in aqueous media leads to phthalocyanine aggregation which their relative concentration depends on type of nanocrystals. In contrast complexes in aqueous media, phthalocyanine aggregation wasn't observed in nanocrystals/ phthalocyanine complexes in DMSO.

Keywords: nanocrystals; quantum dots; quantum rods; tetrapyrroles; photosensitizer; Förster resonance energy transfer; aggregation

Preface

I want to thank Dr. Anna Orlova, Prof. Anatoliy Fedorov, Prof. Alexander Baranov and all my colleagues from the department of Optical Physics and Modern Natural Science in ITMO University.

Very grateful to Prof. Ilkka Tittonen and Prof. Markku Sopanen for their invaluable contribution

Contents

Symbols and abbreviations

Symbols

d	nanostructure core diameter
λ	wavelength
ε	Molar extinction coefficient
q_{0D}	Luminescence quantum yield
I	Luminescence intensity
D	Optical density
E_g	energy gap
μ_h / μ_e	effective mass
h	Planck constant
ν	frequency of radiation
k_{ET}	energy transfer rate constant
R_{DA}	distance between the donor and acceptor
R_0	Förster radius
Φ^2	orientation factor
E	FRET efficiency
τ_{DA} / τ_D	average luminescence lifetime

Abbreviations

NC	nanocrystal
QD	quantum dot
QR	Quantum rod
PC	phtalocyanine
PDT	Photodynamic therapy
FRET	Forster resonance energy transfer
TOPO	trioctylphosphine oxide
DMSO	dimethyl sulfoxide

Chapter 1. Introduction

Relevance of the study. The research of nanotechnology and nanostructured materials is gaining a lot of popularity in the modern world. Lately the studies of semiconductor nanocrystals (NC's), particularly quantum dots (QD's) and quantum rods (QR's) are actively carried out. The sizes of nanocrystals range typically from 2 to 10 nm. Due to the quantum confinement effect, nanocrystals possess unique optical and luminescent properties [1]. The emission wavelength of the luminescence changes as a function of the size of nanocrystals. Because of such properties as the wide absorption spectrum, tunable color emission, optical and chemical stability, the quantum dots and quantum rods are superior to existing organic fluorophores. During the last twenty years, there has been a lot of research activity related to the study of physical mechanisms of QD's interacting with organic photosensitizers (PS's) for photodynamic therapy (PDT) of cancer [2]. By now quite a limited number of studies regarding the complexes of QR's with PS's are known, nevertheless QR is characterized by a high molar coefficient and a large surface area, which allows us to expect that they can be more attractive for biomedical applications as efficient donors of energy and carriers of drugs compared to QD's. PDT is a relatively new method for the treatment of cancer cells. Currently used PS's have properties to accumulate in cancerous tumors and under illumination to generate singlet oxygen, which leads to the destruction of the damaged tissues [3]. Despite the fact that these molecules are used in PDT, they have several disadvantages, e.g., cytotoxicity, long-term excretion, etc. NC/PS complexes could potentially increase the efficiency of the treatment. Nanocrystals as energy donor represent in this case an effective way of transfering energy of the photoexcitation to the acceptor (PS) via the Förster resonance energy transfer (Fig. 1). The use of nanocrystals as energy donors might increase the production of singlet oxygen molecules, as well as to broaden the spectral range of the exciting radiation of the molecules.

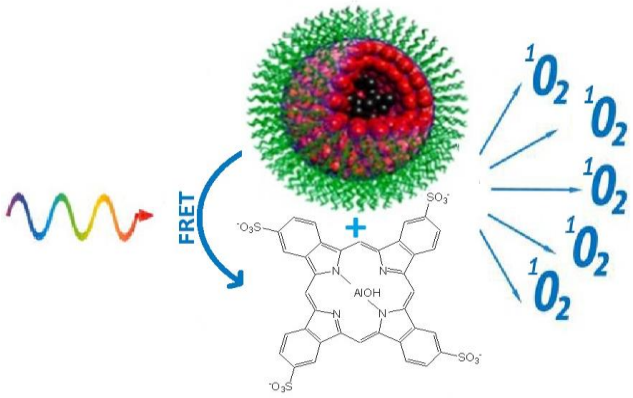

Fig. 1. The system consisting of a quantum dot – an organic molecule of the photosensitizer with effective generation of singlet oxygen.

The aim of this thesis is to find out how the photophysical properties of semiconductor nanocrystal complexes with sulfophthalocyanine molecules depend on the shape and size of nanocrystals.

Chapter 2. Literature review

2.1 Properties of semiconductor nanocrystals

2.1.1. Semiconductor nanocrystals. Quantum confinement effect

Semiconductor nanocrystals or "artificial atoms" are objects which can vary from 1 nm to more than 100 nm depending on the material. By now there are several varieties of nanostructures that differ in size and shape: quantum wells, quantum rings, quantum wires, quantum discs, quantum rods and quantum dots [4]. The main advantage of semiconductor nanocrystals, unlike bulk semiconductors, is that the optical properties depend directly on the size of the object. The dimensional dependence of semiconductor nanocrystals was discovered thirty-five years ago. For the first time nanocrystals were synthesized by the Soviet scientist Yekimov. It is proved in his work [5] that he was able to grow nanocrystals in a transparent dielectric matrix (silicate glass), made up of two components – copper (Cu) and chlorine (Cl). As a result, it was found that the energy spectra showed a blue shift in the exciton bands due to the quantum confinement effect. This effect is present if the geometric dimensions of nanocrystal are commensurated with the de Broglie wavelength of the charge carriers. Therefore, in the structures with reduced dimensions, under the excitation of charge carriers, the electrons and holes become mobile in a space that is confined by potential barriers, and thus one can observe the quantum-confinement effect. If the confinement space is restricted in one direction only, the result is the two-dimensional structure – a quantum well (Fig. 2.1.b). As a result of two-dimensional restriction of space we end up having so called quantum wires (Fig. 2.1.c). Finally, if the motion of electrons, holes and electrons are restricted in all three directions, we have quasi-zero-dimensional systems, quantum dots (Fig. 2.d). These quantum structures are shown in Fig. 2.1. This figure shows that the density of states due to the energy quantization changes radically with respect to the particular effective dimension of the structure. The charge carriers show in quantum dots a discrete energy spectrum in contrast to bulk semiconductors, which correspond to the continuous energy spectrum [6].

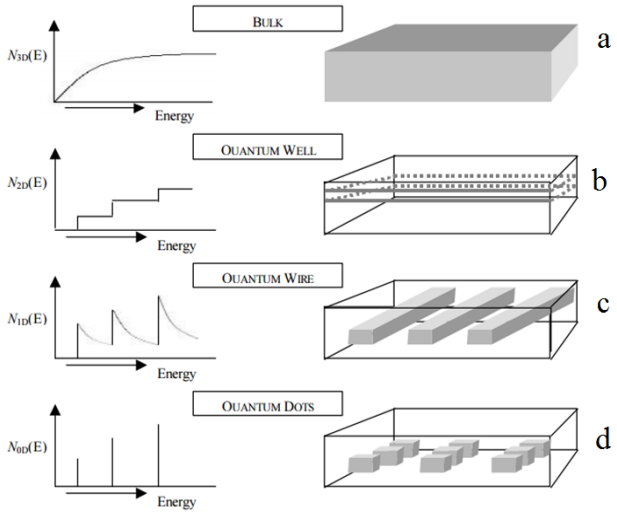

Fig. 2.1 Schematic representation of the structures and dependence of state density of energy in a bulk semiconductor(a) and nanocrystals (b-d) [7].

To obtain the energy spectrum of electrons and holes, it is necessary to solve the Schrödinger equation. Consider spherical nanocrystals, namely quantum dots, surrounded by infinite potential barriers. As follows from equations 2.1 and 2.2, one can find the energy levels of charge carriers and the equation 2.3 shows the energy of the entire system:

$$E^e = E_g + \frac{\hbar^2}{2\mu_e}\left(\frac{\varphi^2_{n_e,l_e}}{R^2}\right) \qquad \textbf{2.1}$$

$$E^h = -\frac{\hbar^2}{2\mu_h}\left(\frac{\varphi^2_{n_h,l_h}}{R^2}\right) \qquad \textbf{2.2}$$

$$E = E^e + E^h = E_g + \frac{\hbar^2}{2\mu_e}\left(\frac{\varphi^2_{n_e,l_e}}{R^2}\right) + \frac{\hbar^2}{2\mu_h}\left(\frac{\varphi^2_{n_h,l_h}}{R^2}\right) \qquad \textbf{2.3}$$

where *Eg* is energy gap, *n* is principal quantum number, which determines energy of the charge carriers at a certain level and *l* is the angular momentum, which determines the shape of orbitals in an atom, respectively. *R* is the radius of nanocrystal, and $\varphi_{l,n}$ is the n^{th} root of spherical Bessel functions ($\varphi_{0,0} = \pi$, $\varphi_{1,0} \approx 4.49$, $\varphi_{2,0} \approx 5.76$, $\varphi_{0,1} \approx 2\pi$ are functions for four lowest energy levels), and μ_e and μ_h are effective mass of an electron and holes (that varies depending on semiconductor material), $\hbar$ is Planck's constant. From Equation 2.3 it is clear that the energy level will increase with a decrease in the size of nanocrystal.

2.1.2 Methods for the synthesis of semiconductor nanocrystals

The first synthesis of nanocrystals was about thirty-five years ago. Since that time scientists have developed completely new methods for synthesis of NC's. Today two fundamentally different approaches to synthesize nanocrystals are widely used: top-down and bottom-up technologies.

Technological process of "top-down" approach is formating of NC's in the processing of macro-scale object or structure and gradually reducing the size of the object to obtain the desired nanometer range. Examples of this approach are photolithography, X-ray lithography and nanolithography. Nanolithography method is present if only nanoparticles are obtained. In this case, the formation of nanoparticles will occur as a result of etching the surface of the material [8, 9].

Examples of "bottom-up" approach are the method of molecular beam epitaxy, the organometallic synthesis of colloidal nanocrystals, the methods of self-organization, etc. [10, 11]. Figure 2.2 presents the colloidal solutions of semiconductors CdSe/CdS quantum dots using organometallic synthesis.

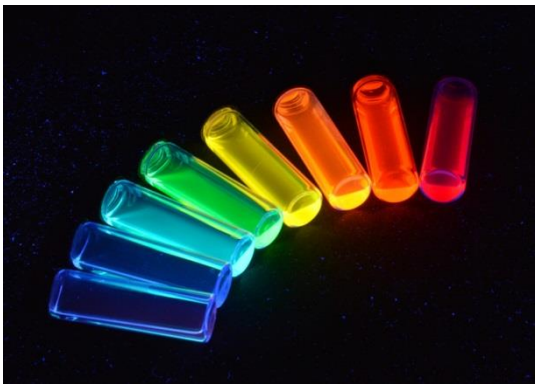

Fig. 2.2 Colloidal solutions of CdSe/CdS quantum dots with different diameter under UV radiation [12].

The typicall materials for the synthesis of nanocrystals consist of the semiconductors $A^{II}B^{VI}$, $A^{IV}B^{VI}$, $A^{III}B^{V}$ groups of Mendeleev's periodic table. In 1993 the scientists at the Massachusetts Institute succeeded to make a significant breakthrough in the synthesis of high quality colloidal quantum dots [13]. They have developed the method for high-temperature synthesis of colloidal quantum dots, combined with pyrolysis of organometallic precursors. Thus, they were synthesized CdSe nanocrystals with high emissivity and narrow size distribution of the nucleus, about 5 %.

Lately, there has been extensive studies of quantum nanostructures of the type $A^{II}B^{VI}$, covered with a thin layer of a semiconducting shell, which acts as a passivating surface for NC's. Composite quantum nanostructures, like core/shell, show new properties compared to quantum dots without the shell. Therefore, making them is an interesting subject to study from the fundamental and practical points of view. In order to shell was uniform around the nucleus is preferably used material which have a similar crystal structure. Otherwise will appear defects at the interface between two phases of shell and nucleus. For example, it is shown in [14] that the synthesis of CdSe quantum dot with intense luminescence. It is succeeded by covering ZnS shell that have a band gap larger than CdSe nucleus. The coatings contributed to the increase of luminescence quantum yield in quantum dots. As can be seen from Fig. 2.3, the photoluminescence intensity increased significantly in quantum dots coated with ZnS shell.

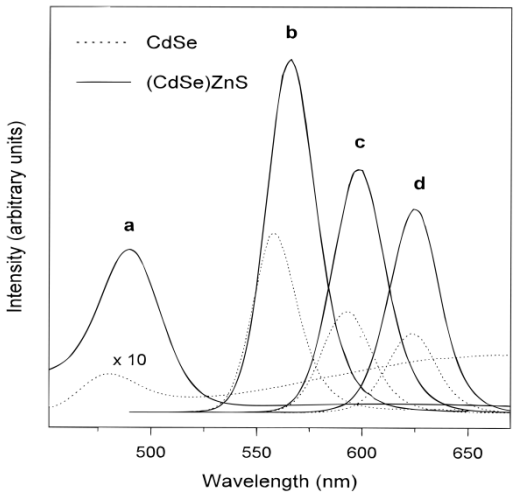

Figure 2.3. The photoluminescence spectra of quantum dots without CdSe shell (dotted graph) and with shell CdSe/ZnS (solid graph) at different core diameter QD[14].

2.1.3 Optical properties of semiconductor quantum dots and quantum rods

As indicated above, nanocrystals show unique optical and luminescent properties due to the quantum confinement effect [1, 15]. As shown in Fig. 2.4, the wavelength of luminescence changes as a function of the size of nanocrystals. Absorption a photon can be a result of the excitation of nanocrystals if the energy exceeds the band gap. In the energy diagram (Fig. 2.4 a), the transition from the ground state to an excited state corresponds to the long-wavelength band in absorption spectra. The luminescence of quantum dots occurs as a result of the transition of the absorbed photon of quantum dot from the lowest excited singlet state to the ground state.

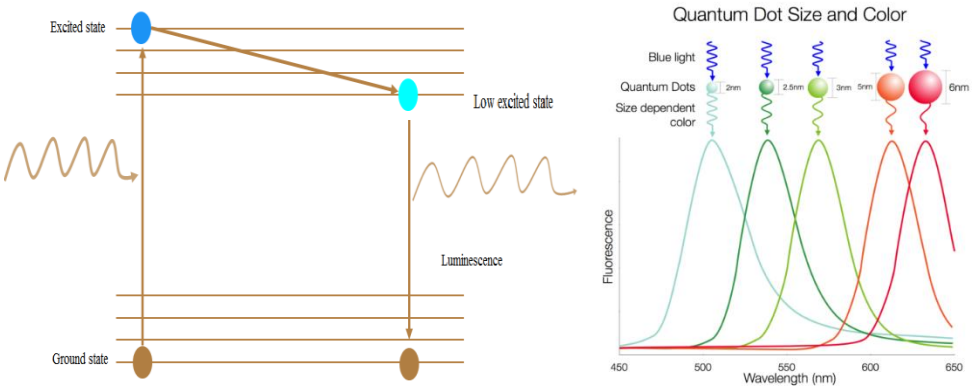

a **b**

Fig 2.4. The energy diagram (**a**) and the dependence of the wavelength on the diameter of the quantum dots with light excitation (**b**) [16].

Due to the extended absorption spectrum, optical and chemical stability and the possibility to "manage" the emission wavelength, the quantum dots and the quantum rods are superior to existing organic fluorophores. These properties make colloidal NC's promising as biological applications and optoelectronic devices.

2.1.4 Practical use of semiconductor nanocrystals

Thanks to the research over the last decade, physical and chemical properties of nanostructures, a wide range of possibilities of potential applications of semiconductor nanostructures have been discovered. The ability to control optical properties by varying the diameter of the NC is considered to be one of the main advantages. In addition, one more advantage of NC's is their property to exist as a colloidal solution. The NC's have been applied in many fields of science and industry, biomedicine, electronics and energy [17]. For example, the practical use of NC's in biomedicine include: fluorescent labels, drug carriers [18, 19], biosensors [20], and biocompatible complexes of nanostructures with photosensitizers for the treatment of cancer diseases by the method of photodynamic therapy (PDT) [21, 22]. Figure 2.5 shows possible applications of the nanocrystals in biomedicine.

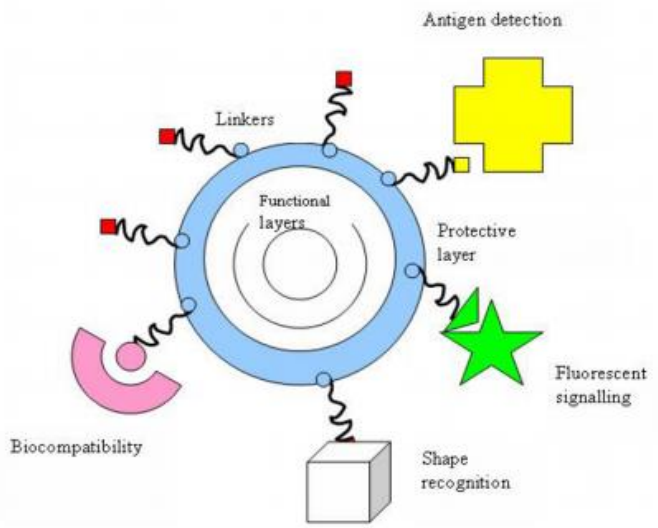

Fig. 2.5. Functional applications of the nanocrystals [22].

2.2 Tetrapyrrole molecules

2.2.1 Using tetrapyrrole molecules in medicine

In recent years, a class of tetrapyrrole molecules (TM) have been of great interest in biomedicine [23, 24]. TM can include such substances as porphyrins, phthalocyanines and chlorins. They represent a heterocyclic group of organic compounds consisting of four pyrroles (aromatic component), interconnected by a carbon bridge. Phthalocyanines (PC's) are well known as photosensitizers for PDT of cancer cells [24]. Modern treatment of cancer tumors includes invasive methods such as surgery, chemotherapy and radiotherapy [25, 26].

2.2.2 Operating principle of photodynamic therapy

Photodynamic therapy (PDT) is an alternative method for the cancer treatment, comprising the use of special drugs – photosensitizing agents. Methodology of PDT involves the injection of a photosensitizer (PS) into the human body, then under the action of light due to the photochemical reactions light is being radiated (Fig. 2.6) [27].

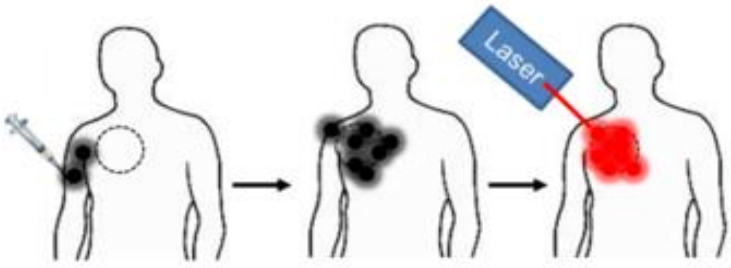

Fig. 2.6 Operating principle of the photodynamic therapy method.

In Fig. 2.7 the mechanism of singlet oxygen generation by photosensitizer is shown. The photon absorption by the photosensitizer is a transition from the ground singlet state (S0) to an excited singlet state (S1). As a result of nonradiative decay of carriers, the metastable triplet level (T1) is being settled and the radiative transition takes place to the state S0 resulting to the emission of a photon. In addition, when the PS is in the triplet state, the molecules of PS participate in photochemical reactions and interact with the molecular oxygen, thereby generating O_2singlet oxygen (Fig. 2.7). In order to achieve high therapeutic activity, the PSs must correspond to several requirements: (1) absence of toxicity in the dark; (2) high selectivity of sensitizer accumulation in tumor; (3) rapid excretion from the body; (4) high quantum yield of singlet oxygen generation; (5) stability in aqueous solutions; and (6) stability under light emission.

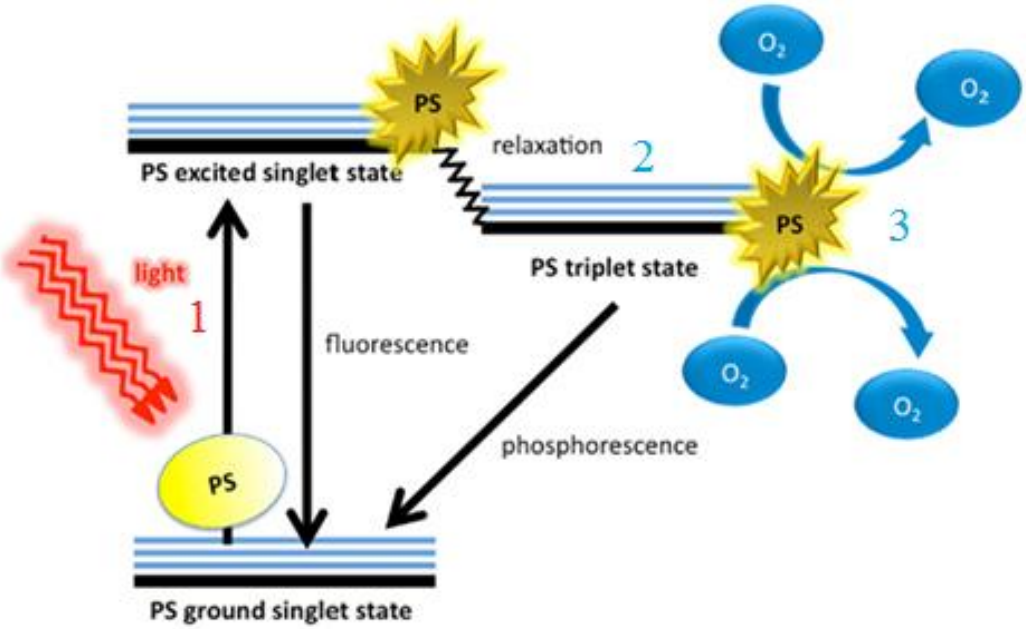

Fig. 2.7. Schematic illustration of singlet oxygen generation. (1) Absorption; (2) transition to the triplet state (intercombination conversion); and (3) nonradiative energy transfer from the PS to the oxygen molecules and O_2generation[28].

2.3 Interaction mechanisms of semiconductor nanocrystals with tetrapyrrole molecules

One of the most important things in the formation of complexes between semiconductor nanocrystal and tetrapyrrole molecule is the mechanism of interaction. Nowadays different approaches are in use for the formation of complexes of nanocrystals with tetrapyrrole molecules (Fig. 2.8): the use of bifunctional ligands, due to hydrophobic forces and covalent chemical bond, as well as the formation of nanocrystals/tetrapyrrole molecule complexes via electrostatic interaction (Coulomb force of attraction). Each of the binding type shows its own characteristics, which may affect physical and optical properties of tetrapyrrole [29].

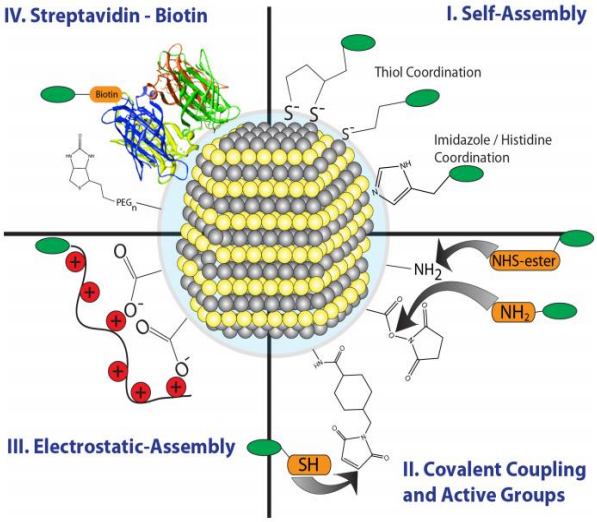

Fig. 2.8. An overview of various binding approaches of NC with TM [30].

2.3.1 Electrostatic interaction

Electrostatic interaction is rather simple and convenient. In this case, negatively charged nanocrystals bind to positively charged tetrapyrrole molecules, or vice versa. For example, it is studied in [31] that CdTe quantum dots, coated with thioglycolic acid (TGA) and 2-mercaptoethanol and negatively charged molecules of phthalocyanine are dissolved ethanol. The main objective of this work was to study photophysical properties of the quantum dot complexes with molecules of photosensitizer with different molecular structure (metal complexes Zn-(tetracarboxy)phthalocyanine (ZnTCPc), Zn-(octabox)phthalocyanine (ZnOCPc) and Zn- (tetrazolo)phthalocyanine (ZnTSPc)). Evaluating the efficiency of intracomplex energy transfer, in case of CdTe/ZnTSPc complexes was about 30%, that is significantly higher compared to CdTe/CdTe and ZnTCPc/ZnOCPc complexes. However, as it has been shown in recent studies [32], with electrostatic interaction in complexes between QD CdTe and Al- (tetrasulfo)

phthalocyanine one can observe changes in the spectral shape of phthalocyanine. Another situation was mentioned in [33]. In this work, there was a study of the optical properties of water-soluble QD CdTe binded with 2-aminoethanethiol with meso-Tetra(4-sulfophenyl)porphin (TSPP), which was formed as a result of electrostatic interaction. Analysis of spectral data showed that in the absorption spectra of porphyrin molecules in the complex with QD, there is a shift and broadening in the Soret band, which was not observed in free porphyrin. It was also shown that these complexes are able to effectively generate singlet oxygen.

2.3.2 Covalent bonding

Covalent binding in NC/TM complexes is usually based on the interaction between the functional carboxyl groups and amino groups. This covalent binding approach is considered to be the most stable, but, also time-consuming process. Advantages of this type of binding can be identified as a high degree of complexes stability, complete absence of their dissociation under normal conditions and rather rigidly fixed distance between NC's and TM's in the complex. Disadvantages are relative labor intensity of obtaining complexes, restriction of choice of research objects (the need for amino function at NC's and carboxyl group at TM's). For example, in [34] the authors studied complexes of CdTe quantum dots, solubilizing mercaptopropionate (TPA) and thioglycolic acid (TGA) with indium and zinc by metal phthalocyanine complexes. Covalent binding occurred using standard linkers: carbodiimide N-ethyl-N-(3-dimethylaminopropyl) carbodiimide and N-hydroxysuccinimide (NHS). It was noticed that by covalent binding there was a displacement of the absorption spectrum of phthalocyanine (approx ~ 2 nm). As the authors stated, the shifts in the absorption spectra characterise this type of bonds and they are caused by the long chain length of the linker between the QD and phthalocyanine molecules.

2.4 Photophysical processes in semiconductorcomplexes of nanocrystals with tetrapyrrole molecules

2.4.1 Nonradiative resonance energy transfer in complexes of semiconductor NC's with organic molecules

Förster resonance energy transfer (FRET) is the mechanism of nonradiative energy transfer, which is carried out by dipole-dipole interaction between a donor molecule in an excited state and an acceptor molecule in the ground state [35]. Donor (D) absorbs the energy as a result of light excitation and then transfers it to the acceptor (A), which is located at a very close distance.

$$D + h\upsilon \rightarrow D^*$$
$$D^* + A \rightarrow D + A^*$$
$$A^* \rightarrow A + h\upsilon$$

where *h*, *v* is Planck constant and frequency of radiation

Illustration of the process of nonradiative energy transfer in donor-acceptor pair is demonstated in Fig. 2.8. In the NC/TM complexes, tetrapyrroles act as acceptors and nanocrystals are donors of energy.

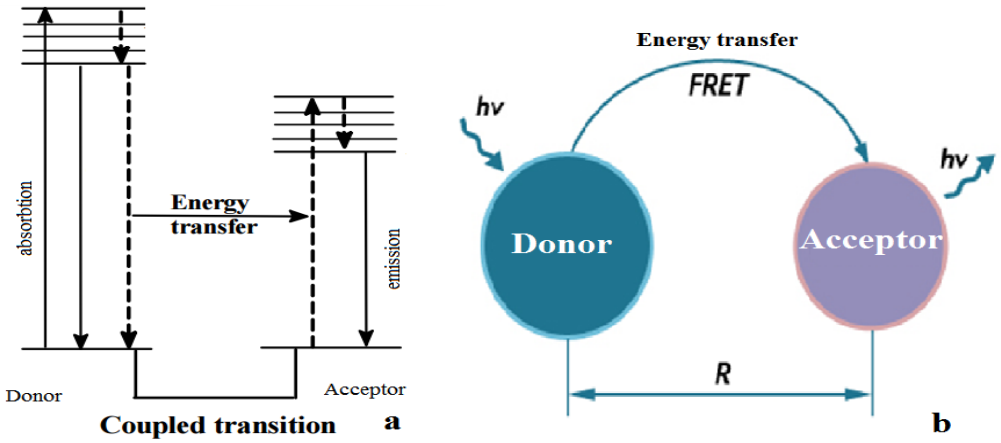

Fig. 2.8. The mechanism of FRET in "donor-acceptor" system on the example of Jablonski energy diagram (a) and the schematic representation of FRET (b).

The result of the energy transfer is the luminescence quenching of the donor and the appearance of sensitized luminescence of the acceptor.

The process of energy transfer in the system "donor-acceptor" can be divided into several steps [36]:

1) energy absorption by the donor (NC's) with the transition to the excited level;

2) vibrational relaxation in the excited state before the establishment of thermal equilibrium with the environment or internal conversion to a stable excited electronic state;

3) excitation energy transfer to the acceptor (TM's);

4) vibrational relaxation in the donor;

5) radiation or degradation of the energy in the acceptor (TM's).

In accordance with the Förster theory in order to perform energy transfer, several conditions must be valid:

— The distance between the donor and acceptor should not exceed the critical radius R_0 (Förster radius). At this distance, the probability of energy transfer FRET is 50%. The typical range of the critical radius R_0 for donor-acceptor pairs ranges from ~1 to ~10 nm [37];

— The overlap integral between the luminescence spectrum of the donor and the absorption spectrum of acceptor should be significant (Fig. 2.9);

— The relative orientation between the dipoles of donor and acceptor should be approximately parallel to each other.

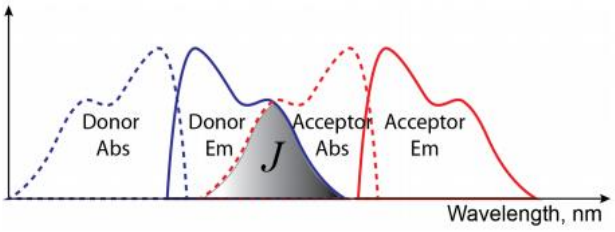

Fig. 2.9. Schematic representation of the spectral overlap integral (gray area), where the luminescence spectra of the donor overlaps the absorption spectrum of the acceptor [38].

Förster obtained the following expression for the energy transfer rate constant k_{ET} [35] :

$$k_{ET}(R) = \frac{1}{\tau_D}\left(\frac{R_0}{R_{DA}}\right)^6, \qquad \textbf{2.4}$$

where R_{DA} is the distance between the donor and acceptor and τ_D is the average lifetime of the donor in the absence of acceptor. The value of R_0 for the selected donor-acceptor pair could be determined from the following relation [35]:

$$R_0^6 = \frac{9000\ln 10 \times \Phi^2 q_{0D}}{128\pi^5 n_r^{\,4} N} \int I_D^H(\nu)\varepsilon_A(\nu)\nu^{-4} d\nu, \qquad \textbf{2.5}$$

where q_{0D} is the quantum yield of the donor luminescence in the absence of the acceptor; Φ^2 is the orientation factor; $I_D^H(\nu)$ is the normalized quantum spectral density

of the donor luminescence ($\int {}_{D}^{H}(\nu)d\nu = 1$), $\varepsilon_A(\nu)$ is the range of molar extinction coefficient of the acceptor; ν is the wavenumber; n_r is the refractive index of the medium; and *N* is the Avogadro constant.

Förster also derived the expression to calculate the theoretical values of energy transfer efficiency, which depends on the critical radius and the distance between the donor and acceptor:

$$E = \frac{1}{1 + \left(\frac{R_{DA}}{R_0} \right)^6}. \qquad \textbf{2.6}$$

The FRET efficiency can also be determined from the formula:

$$E = \frac{k_{ET}}{k_{ET} + k_f + k_r}, \qquad \textbf{2.7}$$

where k_f, k_r are the rate constants of radiative and nonradiative deactivation of the excited state of the donor molecules.

Formula 2.7 is applicable for an isolated donor-acceptor pair, where a single donor interacts with a single acceptor. In a case when a single donor interacts with several acceptors, the expression is converted to:

$$E = \frac{t \cdot k_{ET}}{t \cdot k_{ET} + k_f + k_r}, \qquad \textbf{2.8}$$

where *t* is the number of acceptor molecules that interact with the donor molecule.

Experimentally, the FRET efficiency can be determined from the luminescence quenching of donor luminescence or reducing its average lifetime of luminescence:

$$E_{DA} = 1 - \frac{\varphi_{DA}}{\varphi_D} = 1 - \frac{\tau_{DA}}{\tau_D}, \qquad \textbf{2.9}$$

where φ_{DA} and φ_A are luminescence quantum yields of the donor in the presence and in the absence of acceptor molecules, and τ_{DA} and τ_D are the average average

luminescence lifetime of donor in the presence and in the absence of acceptor molecules, respectively.

Considering the case when the acceptor molecules in complex with a donor are still capable to luminesce, the efficiency of energy transfer can be determined from the formula [39]:

$$E_{DA} = \frac{I_{DA(sens)}(\lambda') \cdot D_A(\lambda'')}{D_D(\lambda') \cdot I_A(\lambda'') \cdot Q}, \qquad \textbf{2.10}$$

where $I_{DA(sens)}$ and I_A are the intensity of acceptor luminescence upon photoexcitation of the donor in the complex and with the direct photoexcitation of the acceptor in complex with donor, D_A and D_D are the optical density of the donor and acceptor at the wavelength of excitation sensitized luminescence λ' and luminescence caused by direct excitation of acceptor, Q is the proportion of donor NC's bonding in the complex with the acceptor molecules.

One of the drawbacks of the formulas 2.6 and 2.9 is that they are not applicable for those cases where during complexing there are additional nonradiative channels of donor deactivation (NC's) and when changing the acceptor characteristics including as luminescence quantum yield in the complexes formation. Therefore, for more correct estimation of FRET efficiency the formula 2.10 is used.

It is known from the literature review that the size and shape of NC's can influence the efficiency of energy transfer in the NC/TM complexes. Currently, however, there is little research work done related to the study of the effect of dimension and shape on the efficiency of intracomplex energy transfer FRET between NC and TM [40]. For example, in [41] NC shape affects the efficiency of energy transfer. The authors believe that since the dipole moment of the QR is different for two axes, the efficiency of energy transfer may depend on the location of dye molecules on the surface of the QR during the formation of complexes, either with the long axis of the QR, or the short one. The dipole moment of NC depends on the size of NC [42], it follows that its change is caused by varying the shape and size of NC. In [43] a linear increase of the dipole moment of CdSe QR with increasing its size is was found. Despite the fact that QR is similar to QD in their optical properties, it is possible to identify a number of differences between them:

— molar coefficient of extinction (molar absorptivity) of QR is by an order of magnitude greater than QD;

— QR has a higher surface area with the same diameter as QD, and, thus, it has a greater number of sites for TM;

— Single QR absorbs and emits linearly polarized light;

— QR has a significantly larger dipole moment, directed along the long axis *c* of the rod [44].

In [41] the dependence of the resonance energy transfer efficiency between CdS NCs and organic dyes, depending on the shape of NC's has been established. In order to better understand the shape effect on the energy transfer efficiency, the fluorescence analysis of QD'sand QR's was carried out with a complex NC in the presence of dye molecules. The experimental energy transfer efficiency was calculated based on the average luminescence lifetime and amounted to 45% and 19% for QD's and QR's, respectively. High efficiency for QD's indicates that the energy transfer from NC's to the dye may be due to different dipole moments of NC.

2.4.2 Photoinduced charge transfer

Luminescence quenching of the donor in NC/TM complexes can be caused by charge phototransfer [45]. Photoinduced charge carriers can participate in the electron transfer in two ways. On Fig. 2.10 the transfer of charge carriers, generated by photoexcitation of QD, is shown: the electron transfer from NC to the lowest unoccupied molecular orbit (LUMO) of the acceptor or the reverse process, the transfer of an electron from the highest occupied molecular orbital (HOMO) of the donor to QD.

As a rule, it several conditions need to be perfomed the carrier transfer: in order to take place energy levels of HOMO and LUMO of TM, or one of these orbitals must be within the band gap of QD; the donor molecules are in close proximity to NC [46-48]. Unlike FRET, the electron transfer rate has an exponential dependence on the distance. At large distances, the electron transfer rate becomes lower than the FRET rate.

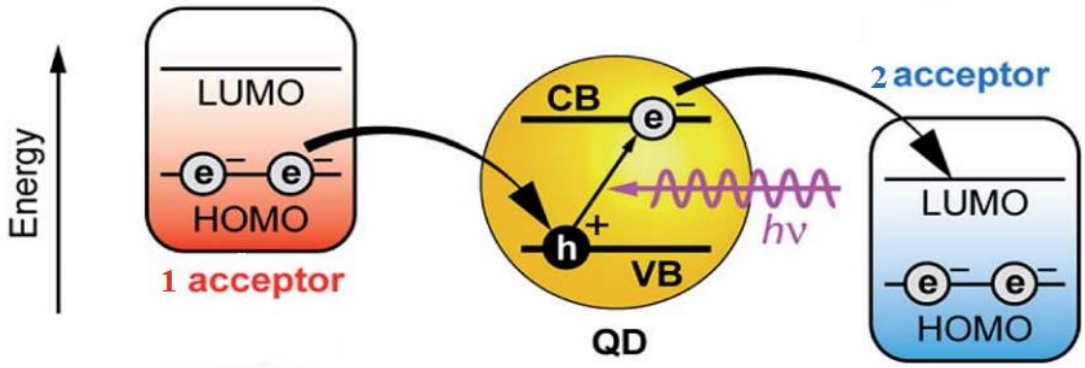

Fig. 2.10. Luminescence quenching mechanism of donor. The dissociation of an exciton generated by photoexcitation of QD. 1 –electron phototransfer from the HOMO of acceptor to the QD, 2 –electrons phototransfer from QD to the LUMO of acceptor [47].

2.4.3 TM aggregation in complexes with NC's

It is known that molecules of phthalocyanine (PC), especially in aqueous media, show a propensity to aggregate [49-52]. The formation of PC aggregates is due to the coplanar binding of TM aromatic rings [53]. The transition from monomer to PC dimer is the result of $\pi - \pi$ stacking between the conjugated phthalocyanine rings [54, 55]. It is also known that PC molecules can form aggregates by binding of a PC central atom (Fig. 2.11 left) and by hydrogen bonding (Fig. 2.11, right). The tendency to PC aggregate depends on many conditions: the type of a PC central atom, the amount of charged sulfonic groups and the solvent polarity. The signs of PC aggregation can be observed in the absorption spectra as hypsochromic or bathochromic shift (shift in band position to a longer wavelength or to a short wavelength) in the spectra[56] and the band broadening. It is also known that formation of PC aggregates can be observed in the complexes with QD's [57]. Due to the formation of PC nonluminescent aggregates in complexes with QD, as there is a decline in the luminescence quantum yield of PC molecules and decrease of the energy transfer efficiency [58], which ultimately can lead to the loss of functional complexes, namely to the ability to effectively generate singlet oxygen.

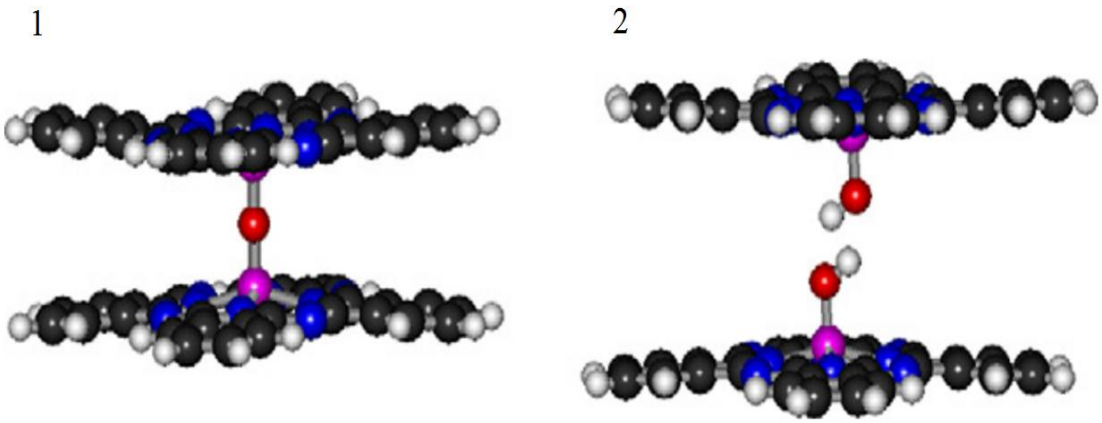

Fig. 2.11 Probable model the formation of dimers as a result of chemical bond: 1 – the chemical bond of the central Al PC atoms by the single bond of oxygen atoms, 2 - by hydrogen bonds [51].

2.5. Conclusions

At present, the study of the semiconductor nanocrystals with organic molecule complexes is an topical subject for research. Based on the literature review, we can conclude that the study of photophysical properties of the nanocrystals/tetrapyrrole molecules complexes are in the focus of many research groups. Despite the large number of studies on this subject, several issues remain debatable. It is known that during the formation of NC/TM complexes, there could be changes in the spectral shapes of acceptor molecules and its photophysical characteristics, due to the significant perturbation of TM's in the formation of complexes. Efficiency loss of NC/PC complexes could be related to the origin of additional competitive channels of nonradiative deactivation of the excited states. However, currently there is no complete conception of the photophysical processes occurring during the migration of photoexcitation energy from NC's to PC's, and the study of regularity of the NC/PC complexes formation are of particular interest.

Thus, the study of the conditions of formation of the TM aggregates in complexes with NC's and study the photophysical properties of complexes depending on the probability of TM aggregates in complexes are important tasks. Solving these problems will help to formulate necessary requirements to the conditions of formation and the stoichiometry of NC/TM complexes, in which the generation of singlet oxygen will be implemented with maximum efficiency for a given D-A pair.

Chapter 3. Methods and materials

3.1. Reagents and materials

In this work, a number of solvents has been used: chloroform, methanol, dimethyl sulfoxide (DMSO) and distilled water, which were purchased from "Neva reagent". Cysteamine was used as molecular stabilizers of NCs, purchased from Sigma Aldrich.

In the study, CdSe/ZnS QD's with a core diameter of 5 nm and QR's with a diameter of 4.5 nm and length of 27.5 nm were used. NC's were obtained as a result of high-temperature organometallic synthesis [14, 59].

The long-wavelength exciton absorption bands of NC's, were observed at a wavelength of 606 nm and 608 nm for QD's and QR's, respectively. The luminescence band maximum was positioned at a wavelength of 625 nm for QD's and 633 nm for QR's, the molar extinction coefficient of QD's was ε=2.2×10^5 M $^{-1}$ cm^{-1} and that of QR's ε = 10^6 M^{-1}cm^{-1} . During the synthesis, the surface of NC's was covered by a layer of trioctylphosphine oxide (TOPO) stabilizer molecules providing NC's solubility in organic solvents. As a result of the phase transfer, QD's and QR's were solubilized by hydrophilic cysteamine molecules to ensure a positive charge on the surface.

An organic component was represented by a drug, "Photosens", which is a mixture of molecules of Al(OH)-sulfophthalocyanine with different degree of sulfonation [60]. The molar extinction coefficient of PC's in the first absorption band was ε = 1,75×10^5 M^{-1}cm^{-1}. The drug "Photosens" was provided by the Federal State Unitary Enterprise "State Scientific Center "NIOPIK".

The luminescence quantum yields of QD's, QR's, free PC's and PC's in QD/PC and QR/PC complexes were determined by a comparative method using Rhodamine 6G in ethanol ($\varphi_{ref} = 0.95$) [61] as a reference:

$$\varphi = \varphi_{ref} \frac{I(\lambda_{exc}) \cdot D_0(\lambda_{exc}) \cdot n^2}{I_{ref}(\lambda_{exc}) \cdot D(\lambda_{exc}) \cdot n_0^2}, \quad \textbf{3.1}$$

where I and I_{ref} are corrected value of area under curve of luminescence spectra for the NC's and the reference sample, respectively; *D* and D_0 are values for the optical densities at the excitation wavelengths of the NC luminescence and the reference sample; n_0 and n are values for the refractive index of the solvent.

3.2. Measurement methods

In this work, the study of NC/PC complexes was carried out using the methods of stationary optical spectroscopy. The absorption spectra of mixed solutions of the QR/PC, QD/PC and free PC's were recorded on a spectrophotometer UV-3600 (Shimadzu) in the visible range of the spectrum.

For the studies of NC/PC, QD's, QR's and PC's luminescence properties, Cary Eclipse spectrofluorimeter (Cary) was used. Recording luminescence spectra was performed the excitation wavelengths of 405 nm, 475 nm and 665 nm. The chosen parameters of the luminescence excitation is due to the fact that at the wavelength of 475 nm, the dominant contribution to the absorption of mixture is created by NC's, and at a wavelength of 665 nm it absorbs only PC's. Luminescence excitation spectra of PCs were obtained by the excitation of the samples at a wavelength of 700 nm. Time-resolved luminescence spectroscopy of the mixed solutions was performed using the laser scanning fluorescence microscope MicroTime 100 (PicoQuant) with the use of an interference filter with a transmission peak wavelength of 670 nm and filter HQ430.

To estimate the average lifetime of NC's luminescence, the average weighted by the amplitude luminescence lifetime were used:

$$\langle \tau \rangle = \frac{\sum_i A_i \tau_i^2}{\sum_i A_i \tau_i}, \qquad \textbf{3.2}$$

where A_i and τ_i are the amplitude and the characteristic relaxation time of the NC luminescence of the *i*-th component.

Data on the average size of NC's were obtained by using a scanning electron microscope (SEM) MERLIN (Carl Zeiss). Imaging was due to Back-scattered Electron Detector (BSE) method. The essence of the method lies in the fact that the detector, integrated into SEM, simultaneously collects backscattered electrons from the sample surface in different directions. The advantage of this method is in recording the contrast images at low values of accelerating voltage from 100 V to 20 kV. SEM images were obtained at an accelerating voltage of 80 kV.

3.3. Phase transfer technique of colloidal semiconductors NC's from the organic to the aqueous phase

To create hydrophilic QD's and QR's, there was the procedure of substitution of the TOPO molecules, stabilized during synthesis by hydrophilic cysteamine molecules (2-mercaptoethylamine hydrochloride). The structural formula of TOPO molecules and cysteamine is presented in Fig. 3.1.

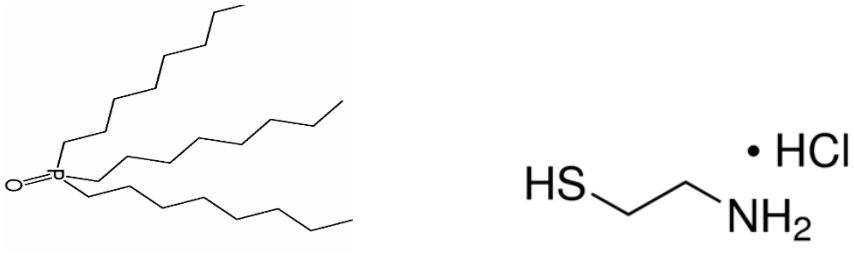

Fig. 3.1 Structural formula of TOPO molecules (left) and cysteamine (right).

To remove the excess stabilizer TOPO from the solution of QD's and QR's, they it was dissolved in an organic solvent (chloroform), then reprecipitated in methanol with the ratio of 1:2. Then an additive of highly concentrated solution of cysteamine in methanol was added to the solution of QD's and QR's. With this cleaning method, up to ~ 95% of organic compounds are removed, in particular, only the organic molecules are adsorbed on the surface of NC's. Thereafter, the resultant mixed solution of QD's and QR's with molecules of the stabilizer was precipitated by a centrifugation for 4 min at 5000 rpm. This resulted in the QD's and QR's being dissolved in distilled water. If after solubilization the solution was transparent and homogeneous, it was considered as a successful stabilizer replacement procedure.

3.4. Technique of sample preparation for electron microscopy

For imaging with a scanning electron microscope, primarily were prepared a low concentration solution of QD's and QR's CdSe/ZnS (~10^{-10} mol/l), coated with a TOPO solubilizer in hexane. After that the microadding of nanoparticles ~ 5 mcl was done and deposited on a carbon substrate. To evaporate the solvent, the sample was placed on a heating plate at a temperature of 40^{o} C. The detection of the samples was done by the collecting of signal secondary electrons, that were reflected from the sample.

Chapter 4. Optical properties of colloidal semiconductor NC's

This chapter presents the optical properties and structural characteristics of colloidal QD's and QR's, obtained with the methods of electron microscopy, the Fourier transform infrared spectrometry and luminescent-absorption spectroscopy.

The main objective of using the technique of scanning electron microscopy, is to determine the shapes and aspect ratios of QD's and QR's. We also carried out an analysis of the vibrational absorption spectra of stabilizer molecules on the NC's surface. In case of colloidal semiconductor NC's, the IR-spectroscopy allows to identify molecules that were adsorbed on the NC's surface. In particular, it is possible to obtain information about what molecules are used as the NC's stabilizer on the surface, and to determine the type of binding to the NC's surface atoms.

4.1 Characterization of quantum dots and quantum rods using electron spectroscopy

Scanning electron spectroscopy (SEM) allows to obtain general information about the shape of NC and to determine the average size and the size distribution in the ensemble. Figures 4.1 and 4.2 show the SEM images of CdSe/ZnS QD's and QR's. Comparing the SEM images, it is clear that NC's are significantly different from each other: QD's have a spherical shape and QR's correspond a cylindrical shape. Only on the basis of SEM images, one could get information about the shape and aspect ratio of NC. It should be noted that if NC's are in the state of aggregation, SEM images provide the data about their aggregation degree [62].

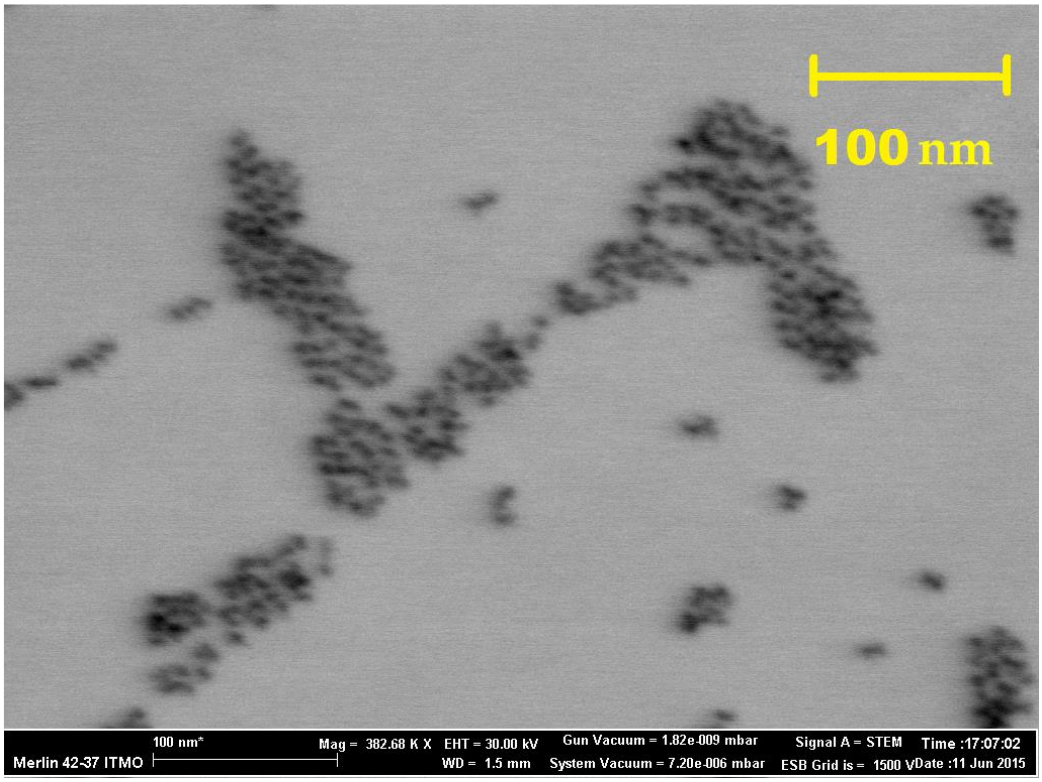

Fig. 4.1. SEM image of CdSe/ZnS quantum dots.

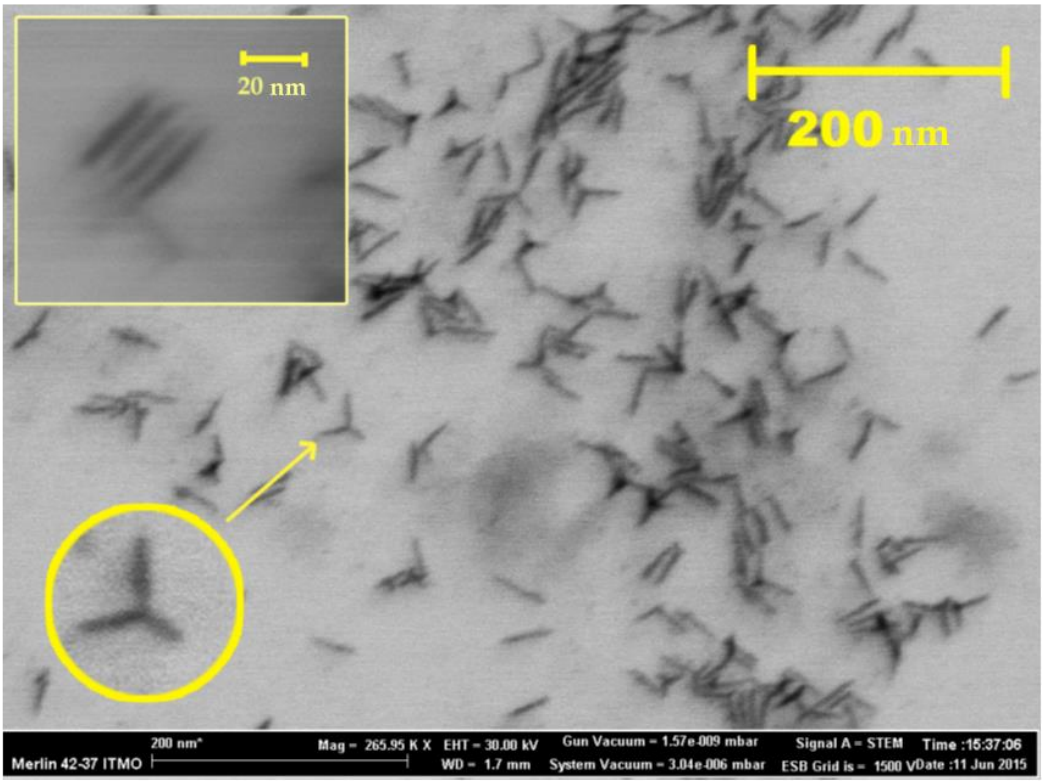

Fig. 4.2. SEM image of CdSe/ZnS quantum rods.

The SEM image of QR's (Fig. 4.2) shows that the vast majority of NC's in the sample has a rod-shape. However, there are also some structures with a tetrapod shape. Also Fig. 3.2 shows an example of QR arranging.

The average NC diameter was determined by the size evaluation of over 60 nanoparticles on the SEM images. Figure 4.3 shows a histogram of the size distribution. Analysis of the data, presented in Figure 4.3 (a and b), showed that the average diameter value for QD was $(5 \pm 0{,}1)$ nm and for QR $(4.5 \pm 0{,}1)$ nm. Special attention was paid to the average length of QR, the size of which was $(27 \pm 0{,}1)$ nm (Fig. 4.3 (b)).

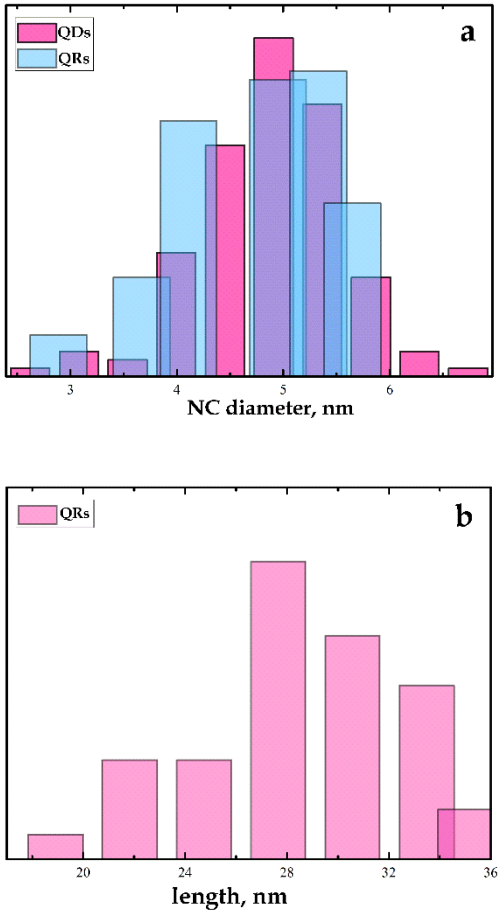

Fig. 4.3. A histogram of NC's size distribution (a) and a histogram of the QR's length distribution (b).

4.2 Characterization of nanocrystals by Fourier spectroscopy methods

In this thesis, carry on analysis of the vibrational absorption spectra of samples with NC's that were coated with hydrophobic and hydrophilic organic stabilizer molecules.The study of IR-spectra of samples was performed, firstly, in order to confirm the substitution of the solubilizer from the hydrophobic (TOPO) to hydrophilic (cysteamine) on NC's surface by the phase transfer from the organic to the aqueous

phase. Secondly, to determine which functional groups of the solubilizer molecules were involved in bond formation between NC's and these molecules.

Figure 4.4 presents the IR-absorption spectra of QD-TOPO and TOPO as a reference spectrum. Having identified the compound from the sample with QD-TOPO by vibrational spectrum and compared it with the position of the absorption spectrum of free TOPO, it should be noted that they are almost identical, except for the hypochromic shift of vibrations band of P=O (~1463 cm^{-1}).

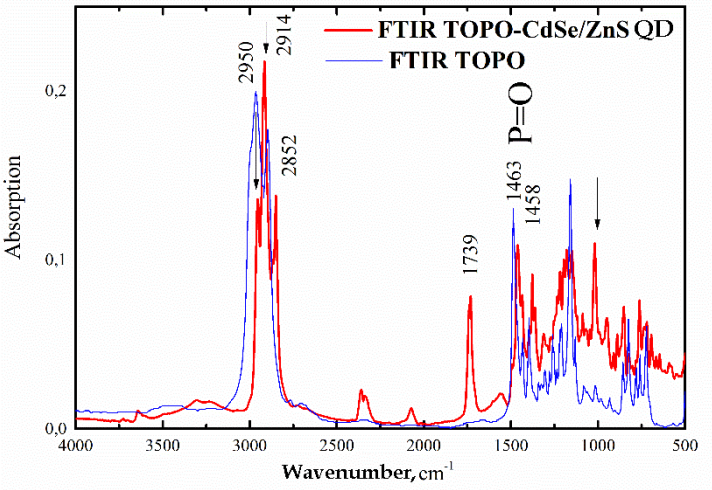

Fig. 4.4. The IR-absorption spectrum of QD molecules (CdSe/ZnS), coated with TOPO molecules and free TOPO.

As can be seen from Fig. 4.5, at the length of 2950 cm^{-1} there is a narrow band corresponding to the –CH3 group of asymmetric stretching vibrations. At the wavenumber ~2914 cm^{-1} and ~2852 cm^{-1} intense narrow bands of symmetric and asymmetric stretching vibrations of the alkyl chains ν(-C-H2) are observed, it indicates the presence of octyl groups of TOPO molecules. Also on the IR-spectrum of CT-TOPO (Fig. 4.4), the narrow band at 1739 cm^{-1} is clearly visible, this indicates the presence of carboxyl group –COOH on the surface of the QD. To check the availability of organophosphorus compounds on the surface of the QD, one should compare an oscillating narrow strip (~1463 cm^{-1}) of stretching vibrations P=O in the spectrum of free TOPO (Fig. 4.4) with the vibrational spectrum of QD-TOPO. It is known from the literature review that for TOPO related molecules with the surface of the QD, the band of stretching vibrations P=O is shifted to the longer lenghts wave in the spectrum [63]. Accordingly, the position of organophosphorus compounds is at the wavenumber ~1458 cm^{-1}, confirming the presence of TOPO molecules on the surface of QDs. It follows, that phosphinate TOPO groups are coordinated to the shell of ZnS QD [64].

Figure 4.5 shows a schematic representation of QD before and after the solubilization process by cysteamine molecules.

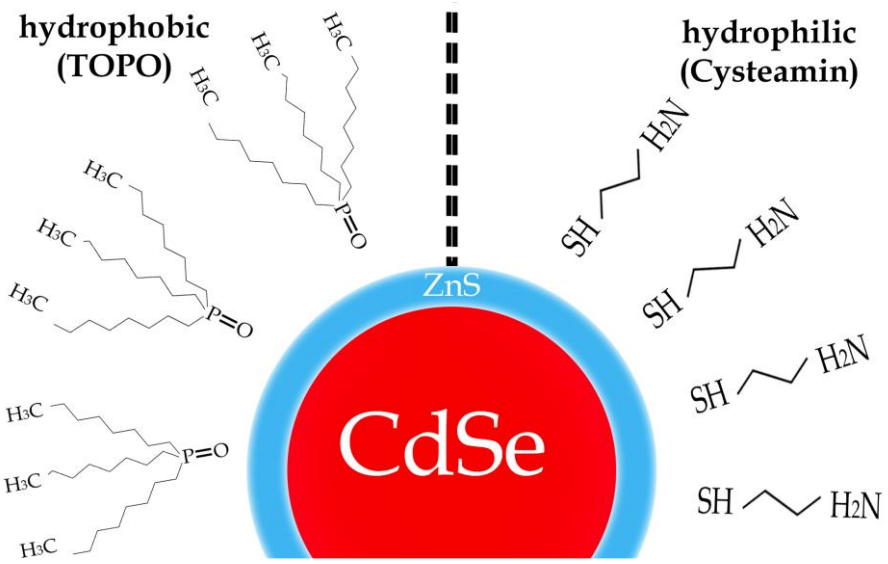

Fig.4.5 Schematic representation of QD, stabilized by hydrophobic and hydrophilic molecules.

As a result of the phase transfer, the substitution of hydrophobic TOPO ligands on the QD surface ligands by hydrophilic cysteamine stabilizer takes place. After the solubilization process, QD's were dissolved in distilled water.

To determine the type of chemical bonds between cysteamine and QD's CdSe/ZnS, an analysis of IR-absorption spectra of QD-free cysteamine and cysteamine was carried out, and presented in Fig. 4.6. According to the structural formula (see Chap. 3, Fig. 3.1), cysteamine molecule contains amino groups (-NH), thiol groups (-SH) and a chain of two methylene groups (-CH2).

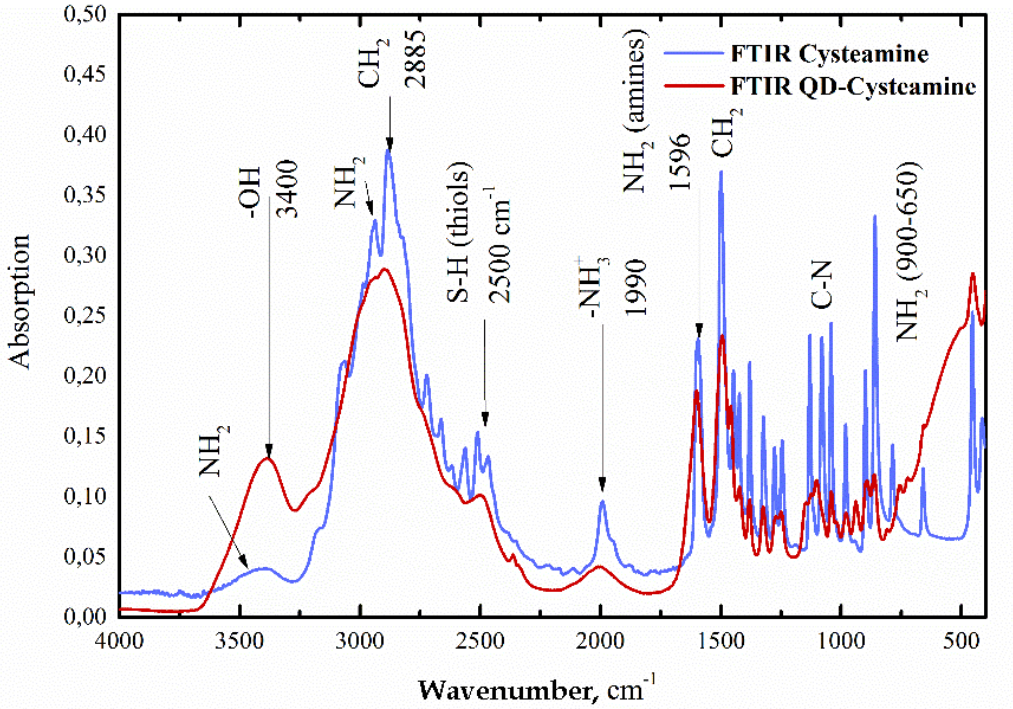

Fig. 4.7 IR-absorption spectra: cysteamine stabilizer and sample of QD-cysteamine.

The absorption of cysteamine at 2450-2600 cm^{-1} is caused by stretching vibrations of the molecules of the thiol group (-SH). On the IR-absorption spectrum of QD-cysteamine in the range of 3700 - 2600 cm^{-1} with a peak at a wavenumber ~3400 cm^{-1}, there are the superpositions of several absorption bands. It is due to the overlapping bands of stretching vibrations of O-H-distilled water (H_2O), and stretching vibrations of N-H (-NH^2) of cysteamine. In the IR-spectra of cysteamine and QD, the narrow band at the wavenumber ~1596 cm^{-1} corresponds to the deformation vibrations of N-H (amino group NH^{3+}). Also the IR-spectrum of cysteamine shows a very broad bands at 2300 and 3300 cm^{-1}, which is responsible for the stretching vibrations of the CH2 bond. One band, located at~2700 cm^{-1}, is observed as a result of binding between cysteamine and hydrochloride (HCl). It is observed from the analysis of IR-spectra of a QD sample that as a result of the solubilization shows a decrease of the band intensity at ~2500 cm^{-1} with respect to the vibrational bands of free cysteamine, which is caused by the stretching vibrations of the thiol group (-SH). It follows that the functional – SH groups of cysteamine are covalently linked to QD's on the surface. It is also known that the thiol groups have a strong electron affinity to zinc in the ZnS shell [65]. This electron affinity describes the tendency of the thiol group to a stable covalent bond with a ZnS shell. This directly indicates a successful substitution of TOPO molecules to cysteamine molecule on the surface of QD [66]. As a result of the solubilization by molecules of cysteamine,

QDs acquire a positive charge on its surface (provided that, if the molecules of cysteamine are protonated). Based on the fact that stabilizer molecules on the surface of QD have a positive charge, it can be assumed that the formation of NC/PC complexes will be implemented as a result of the electrostatic interaction between negatively charged PC sulfonic groups (if there is neutral pH, PC sulfonic groups are dissociated, therefore they, have a negative charge) and positive amino groups of cysteamine on the NC's surface.

4.3 Effect of the nearest nanocrystals environment on their optical properties

The optical properties of NC's before and after the phase transfer, based on luminescent-absorption spectroscopy, were evaluated in this work. Analysis of spectral-luminescent characteristics allows us to determine the effect of replacement of ligands on the NC's surface on their optical properties. Figures 4.7 and 4.8 show the absorption spectra and the luminescence of water soluble CdSe/ZnS QD's and QR's, recorded before and after the replacement of cysteamine solubilizer on their surface.

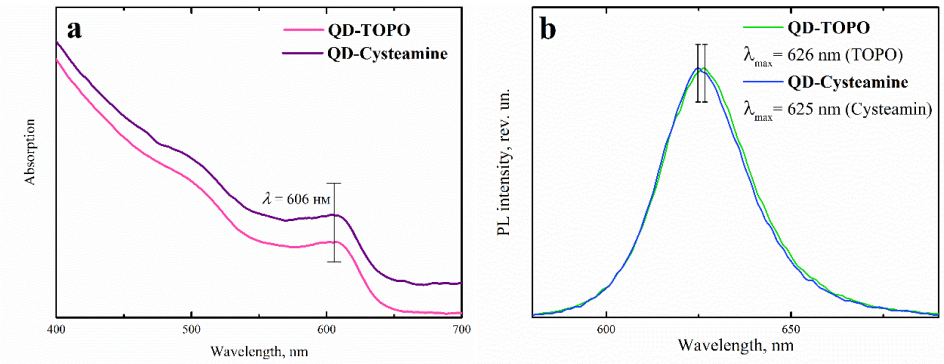

Fig. 4.7 Spectral-luminescent characteristics of CdSe/ZnS QD's of solubilized TOPO and cysteamine: a – the absorption spectra of QD; b – QD luminescence spectra upon excitation by light at a wavelength of 475 nm.

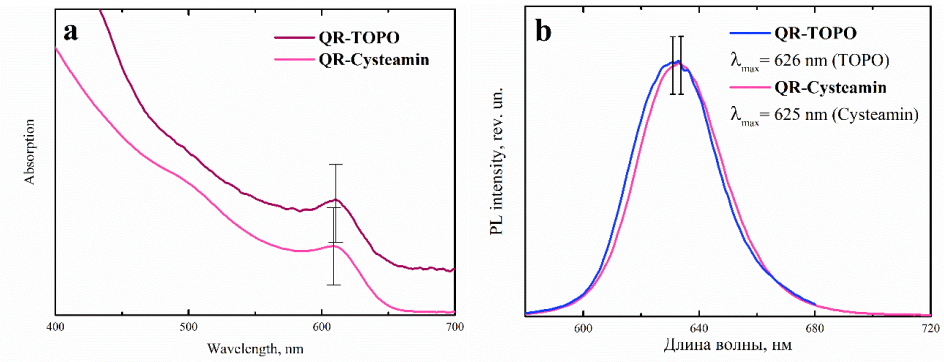

Fig. 4.8 Spectral-luminescent characteristics of CdSe/ZnS QR's of solubilized TOPO and cysteamine: a – the absorption spectra of QR; b – QR luminescence spectra upon excitation by light at a wavelength of 475 nm.

Fig. 4.7 and 4.8 show the replacement of hydrophobic to hydrophilic stabilizer leading to minor changes in the absorption and luminescence spectra of NC's. The spectral-luminescent characteristics of QD's and QR's CdSe/ZnS are shown in Table 4.1. It was found that in the luminescence spectra there is a slight hypsochromic shift for QD's and hypsochromic shift for QR's. We also found an increase in the halfwidth (FWHM) of luminescence band of QD's and QR's after the solubilization of hydrophilic molecules. These changes have resulted in different pH indicators in solutions with samples of NC-TOPO (in hexane) and NC-cysteamine (in distilled water).

Table 4.1 Spectral-luminescent characteristics of NC used in this work.

NC'sType	Stabilizer	Solvent	λ, nm (first exciton position)	λ, nm (max luminescence peak)	FWHM, nm
QD's	TOPO	Hexane	606	626	31
	Cysteamine	Water	606	625	33
QR's	TOPO	Hexane	610	631	39
	Cysteamine	Water	608	633	42

After solubilization by cysteamine, the luminescence quantum yield of QD's decreased almost to half (Table 4.2) compared to the initial value for QD's, coated with TOPO molecules. The reason for the drop is caused by the formation of defects on the shell of ZnS NC's during synthesis. If the shell covers evenly the nucleus of NC, it is possible that the cysteamine thiol groups interact with the nucleus atoms of CdSe NC. In particular, the cause of the quenching of luminescence quantum yield is the phototransfer of a hole from NC to the thiol molecules [67-69]. In contrast to QD's, QR's after the solubilization phase by cysteamine, showed a more stable luminescence quantum yield. This is because QR's are coated with a thicker shell, which reduces the efficiency of the hole phototransfer.

Table 4.2 Luminescent properties of NC's

Nanocrystals type	Solubilizer type	Luminescence quantum yield , %	$\langle\tau\rangle$, ns
QD	TOPO	6	19,3
QR	TOPO	14	-
QD	Cysteamine	3	16,6
QR	Cysteamine	11	12,5

Also the analysis of time-resolved luminescence of QD and QR samples before and after the phase transfer was studied. Average luminescence lifetimes of NC's were approximated with biexponential dependence, the average luminescence lifetimes were determined by the formula (see Chap. 3, Formula 3.2). Along with the drop of the luminescence quantum yield for QD's, the reduction luminescence lifetimes was observed from 19.3 to 16.6 ns.

4.4 Conclusions

Characterization of CdSe/ZnS colloidal quantum dots and quantum rods, was perfomed with the implementation of electron microscopy and stationary optical spectroscopy. This leads to the following conclusion:

1. The NC's ensemble samples, used in this thesis, are characterized by shapes uniformity of the shape of nanocrystals, i.e. QD's are rather to spherical whereas QR's assembly rods. The statistical analysis of SEM images of the samples showed that the samples can be characterized by a small size range, and in the case of QR's there is also a small spread in relation to the diameter of NC's to their length.

2. Analysis of IR-spectra demonstrated that the phase transfer of NC's from the organic phase in the aqueous one makes it possible of which to obtain NC's, surfaces are stabilized by hydrophilic cysteamine molecules. According to IR-spectroscopy, the surface atoms of Zn shell CdSe / ZnS NC's are are covalently linked to by a thiol group.

3. The study of spectral-luminescent properties of colloidal NC ensembles showed that the phase transfer of the samples to aqueous solutions had virtually no effect on the absorption and luminescence spectra of NC's. Herewith, the luminescence quantum yield of NC's, stabilized by cysteamine, was noticeably lower than that of the initial NC's, stabilized by TOPO molecules.

Chapter 5. Study of the formation conditions and optical properties of CdSe/ZnS nanocrystals with PC in aqueous solutions

This Chapter presents the results the study of the formation conditions and optical properties of cationic CdSe/ZnS NC's in complexes with PC organic molecules, formed via electrostatic interaction in aqueous solutions. Below are the results of the effects of size and shape of nanocrystals in complexes with PC on the formation PC molecules of the aggregated type. It is shown that the concentration of nonluminescent PC aggregates in complexes with NC's has a strong dependence on the shape of NC's.

5.1 Optical properties of NC/PC complexes in water solutions

In order to find out the mechanism of the electrostatic interaction, NC's were previously stabilized by hydrophilic molecules of cysteamine, resulting in a positive charge provided on the NC's surface in aqueous solution. The negative charge of PC's was caused by the dissociation of sulfonic groups in distilled water. Formation of complexes occurred by mixing NC's with PC's in an aqueous medium (pH = 7) via electrostatic bonding between the amino groups of cysteamine molecules, adsorbed on the NC's surface and negatively charged sulfonic groups of PC molecules.

In line with the FRET mechanism (see Chap. 2, paragraph 4.1, Formula 2.4-2.6), to carry out an effective energy transfer between QD-PC and QR-PC, there needs to be an overlapping luminescence spectrum between donor (QD's and QR's) with the absorption spectrum of the acceptor (PC's).

Table 5.1 shows the values of the overlap integrals (J), the critical radius (R_0), the distance between the donor and acceptor (R), the value of the energy transfer rate constant (k_{ET}) and the theoretical value of energy transfer efficiency (E_{th}).

Table 5.1 Theoretical estimates of FRET parameters for NC/PC systems

NC Type	Luminescence quantum yield[a], %	J^b, $M^{-1} cm^3$	R_0^c, nm	R^d, nm	k_{ET}^e, c^{-1}	E_{th}^f
QD	3	5.08×10^{-12}	5.52	3.64	1.02×10^9	92 %
QR	11	6.24×10^{-12}	7.1	3.64	2.4×10^9	98%

Calculation of NC's luminescence quantum yield was provided using the formula 3.1 (see Chap. 3). The overlap integral of NC's luminescence spectrum and the absorption spectrum of PC was calculated by the formula:

$$J = \int I_D^H(\nu) \cdot \varepsilon_A(\nu) \cdot \nu^{-4} \cdot d\nu, \qquad \textbf{5.1}$$

where I_D^H is normalized spectrum of NC's luminescence; $\varepsilon_A(\nu)$ is the absorption spectrum of PC molecules; ν is the wave number (cm^{-1}).

The Förster radius (R_0^c) was calculated using formula 2.5 (see Chap. 2, paragraph 1.4). The distance between the donor and acceptor (R^d) was defined as the sum of the NC's radius, ZnS shell thickness and the length of the stabilizer cysteamine molecules. The values of the rate constants of energy transfer (k_{ET}^e) and the theoretical values of energy transfer efficiency (E_{th}^f) were determined by the formulas 2.4 and 2.6 (see Chap. 2, paragraph 1.4).

Figure 5.1 shows the absorption and luminescence spectra of CdSe/ZnS QD's and QR's, used in this thesis, as well as the absorption spectrum of PC molecules. The NC's concentration in NC/PC mixed solutions was constant for QD's ($C_{QD} \sim 10^{-7}$mol/L) and for QR's ($C_{QR} \sim 10^{-7}$mol/L). The shaded area in Fig. 5.1 shows the overlap integral of the spectra of the donor and acceptor. It can be assumed that the implementation of the energy transfer by FRET mechanism in the systems of QD/PC and QR/PC will occur under approximately same conditions, since the values of the overlap integral for QD's and QR's was not significantly different from each other.

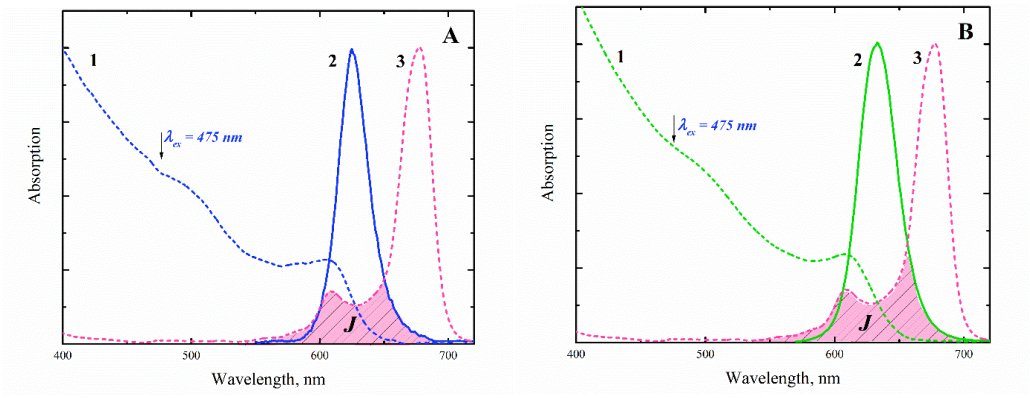

Fig. 5.1 Spectral-luminescent characteristics for QD's (**A**), for QR's (**B**) and PC molecules: NC's absorption spectra of (**1**) and PC (**3**); NC's luminescence spectra of (**2**) when excited with light at a wavelength at 475 nm. The shaded area shows the overlap integral for the of NC/PC complexes.

Figure 5.2 shows the absorption spectra of QD's, QR's and two systems of QD/PC and QR/PC with increasing relative concentration of PCs in the mixed solution $n = C_{PC's}/C_{NC's}$. The relative concentration of PC's ranged from 0.1 to 10. The successive PC's microaddings in an aqueous solution with QD's and QR's on the absorption spectra (Fig. 5.2 A, B), lead to an increase in the intensity of the first Q(I) PC absorption band at the wavelength range of 650-720 nm (Fig. 5.1).

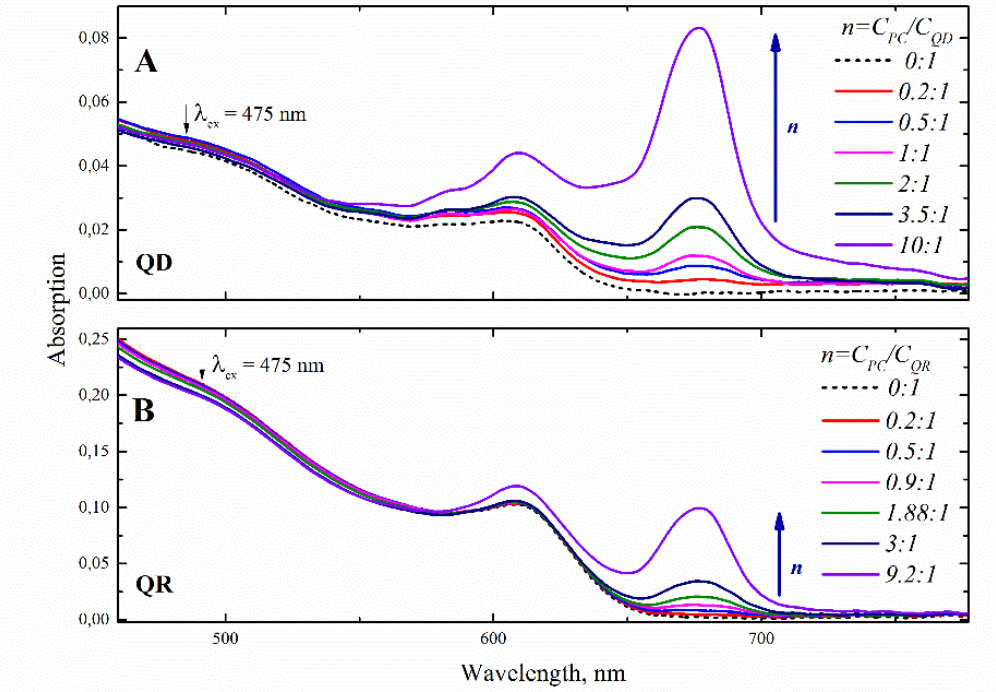

Fig. 5.2. The absorption spectra of the NC's and NC/PC mixed solutions with increasing relative concentration of PC's: A – QD/PC, B – QR/PC.

The absorption spectrum from the NC/PC mixed solutions within the range of 450-550 nm, revealed no changes. Because of this spectral region, there is a "window of transparency" in PC molecules, the contribution to the absorption is caused only by NC's. In the case of NC/PC complexes, the aggregation of PC molecules in combination with NC's is possible. Therefore, to determine whether the PC aggregates are formed in the complexes with NC's, we made an analysis of the absorption spectra obtained from NC/PC mixed solutions. From the absorption spectra of QD/PC and QR/PC mixed solutions the contribution of the absorption spectrum of NC's was subtracted and the differential absorption spectra of PC's was obtained.

Figure 5.3 presents the differential absorption spectra of PC molecules in mixtures with NC's. As a comparison, the absorption spectrum of an aqueous solution of PC's is also shown.

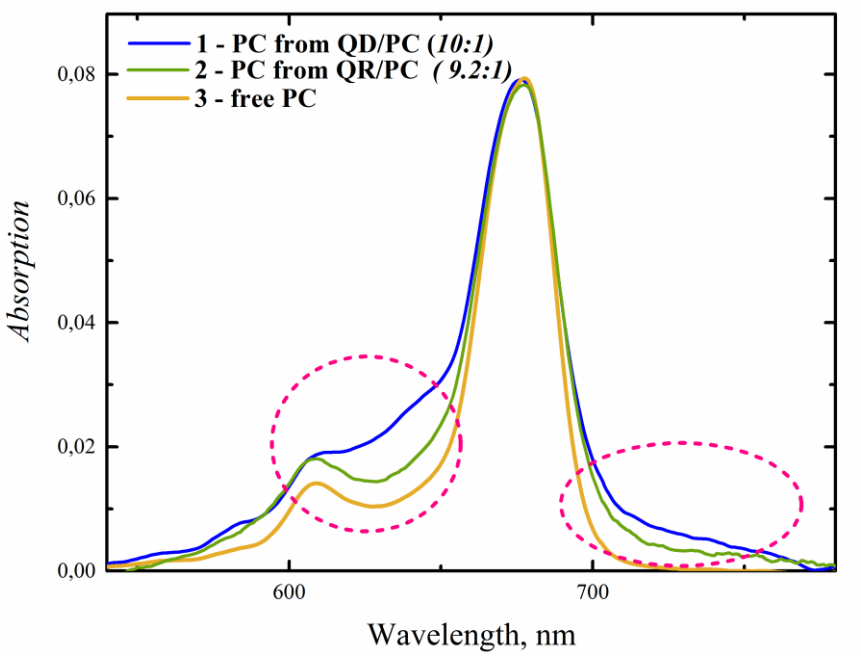

Fig. 5.3. Absorption spectra of PC in solutions with QD's and QR's. Absorption spectra of PC's: differential absorption spectrum of PC in the mixture with QD (**1**), difference absorption spectra of PC's in the mixture of QR's (**2**), absorption spectrum of free PC (**3**) ($C_{PC}=9.4\cdot10^{-7}mol/L$)

When comparing the difference absorption spectra of PCs in mixed solutions with QD's and QR's to the absorption of free PC spectrum, one can find a significant decrease in the intensity of electronic absorption of the Q-band (~ 677 nm) and its corresponding vibrational band at the wavelength (~ 608 nm) of PCs in mixtures with QD's and QR's, there is more pronounced of the mixture for QD's with PC's. Spectral shape variation of difference absorption spectrum of PCs mixed with NCs at a wavelength of 640 nm was also found. It is due to the dimerization of PC molecules in the complexes with QD's and QR's. According to the literature review, the molecules of PC show a tendency to spontaneous aggregation [49-51] in aqueous solutions. Analysis of the absorption spectra of PC's in the mixture with QD's and QR's shows that the absorption spectra of the compounds, shown in Fig.5.3, are not additive sums of components in the mixture. This indicates the formation of PC aggregates in the complexes with NC's. In the differential absorption spectra of mixtures of PC's with NC's and PC absorption spectrum, the concentrations of PC aggregated molecules were determined.

Figure 5.4 shows the dependence of the percentage of molecules in PC agreggates in the complexes with QD's and QR's with increasing of the relative concentration of PC in aqueous solutions.

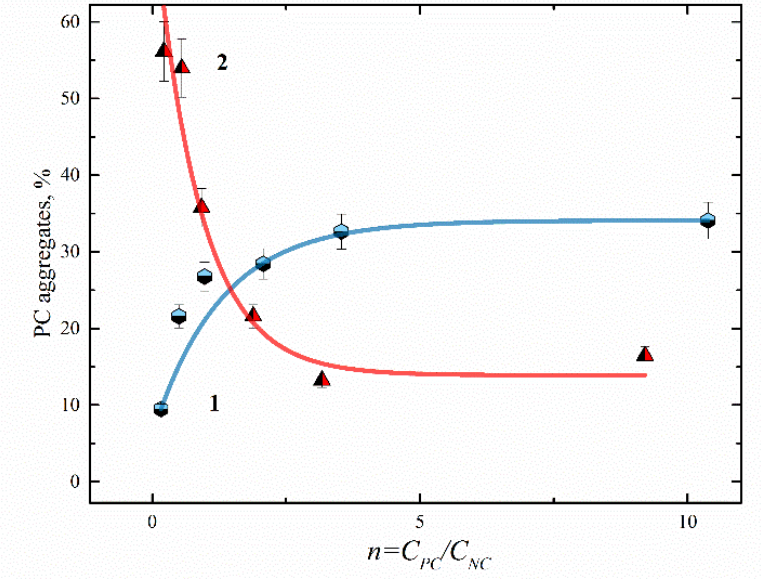

Fig. 5.4 Dependence of the percentage of PC aggregates in complexes with NC's on the relative concentration of PC's ($n = C_{PC}/C_{NC}$) in aqueous solutions: *1*–QD, *2* – QR.

QR's show a large surface area, therefore, they have a greater number of sites for molecules of PC and PC neighboring molecules on the surface of QR may be located at distances larger than at the QD surface. Evaluations showed that about 380 molecules of PC could reach the surface of QR, which is 3.5 times more than in the case of QD (~110). The formation of PC aggregates in complexes with NC is probabilistic in nature. Therefore, it can be assumed that the increase of seats on the surface of NC should lead to a decrease in the probability of PC aggregation in complexes, i.e. in complexes with QR, the relative contents of the aggregates should be lower than in the complexes with QD. Fig.5.4 shows that this assumption is supported by experimental data at relatively large concentrations of PC in the samples. So, starting with $n=3$, the content of aggregates in the samples with QD is up to 30% of the total concentration of PC's, which is 3 times higher than the content of PC aggregates in the samples with QR's. It is necessary to indicate an abnormally large content of PC aggregates (55%) mixed with QR's at low concentrations of PC molecules in the sample. The reason for such a high concentration of aggregates in this case is unknown.

Figure 5.5 presents the luminescence spectra of the mixture QD/PC at different ratios of molar concentrations and the luminescence spectra of QD in the absence of PC molecules (excitation light at a wavelength of 475 nm).

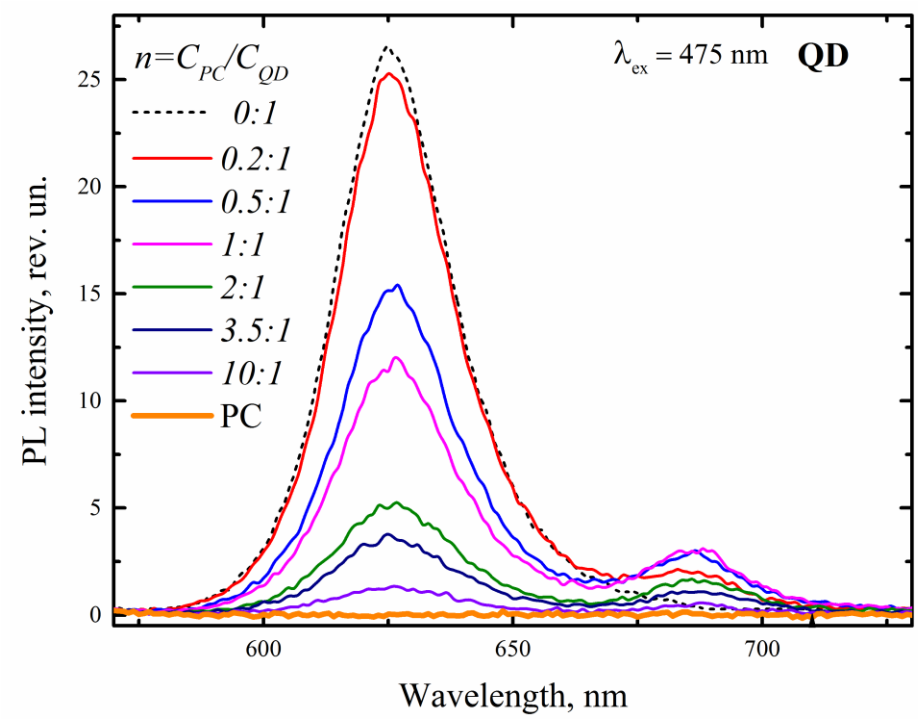

Fig. 5.5 Luminescence spectra of QD and mixed solutions of QD/PC upon excitation by light at a wavelength of 475 nm.

Fig. 5.5 shows that with an increase of the relative concentration of the acceptor molecules in the complexes of QD/PC, the effective luminescence quenching of QDs (max 631 nm band) is observed. Fig. 5.5 reveals that the appearance of the strip in the area of 686 nm corresponding to the luminescence of PC. As shown from Fig. 4.5 (orange line) at excitation of free PC molecules by light at a wavelength of 475 nm luminescence is not observe. This implies that the quenching of the luminescence of the donor and the appearance of sensitized luminescence band of PC indicate the photoexcitation energy transfer between donor (QD) and acceptor (PC), which could only be implemented under conditions when formed complexes.

One can note that with increasing the relative concentration of the acceptor molecules, the intensity of sensitized luminescence starts to increase, but at values higher than the molar concentration ratio of 1: 1 it gradually diminishes.

A similar pattern is observed in the case of QR/PC complexes (Fig. 5.6). Analysis of the luminescence spectra of QR's shows the effective luminescence quenching of QR's as a result of the energy transfer to PC's. One can see from Fig. 5.6 that in the luminescence spectra of the of QR/PC complexes, there is the presence of sensitized luminescence PC (maximum band is ~ 686 nm) even in the case of QD/PC complexes.

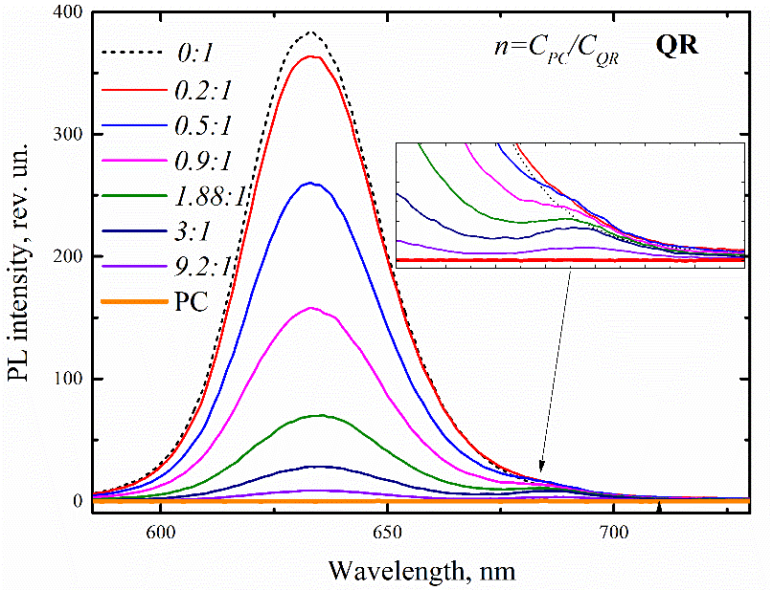

Fig. 5.6 Luminescence spectra of mixed solutions of QR/PCand QR in free shape, under light emission at a wavelength of 475 nm.

5.2 Photophysical properties of NC/PC complexes in aqueous media

Analysis of the experimental dependences of the relative luminescence intensity of NC I/I_0 (I, I_0 is the intensity of NCs luminescence in the presence of PC molecules and in their absence, respectively) on the relative concentration of PC molecules (the so-called quenching curve) allows us to obtain information about the average number of acceptors, coupled in a complex with a single donor. If one acceptor molecule completely quenches the luminescence of the donor in the complex, it is also possible to estimate the fraction of donors, which could be associated with the acceptor molecules in the mixed solution. The dependences of the relative luminescence intensity of NCs on the relative concentration of PC molecules (n) are shown in Fig. 5.7.

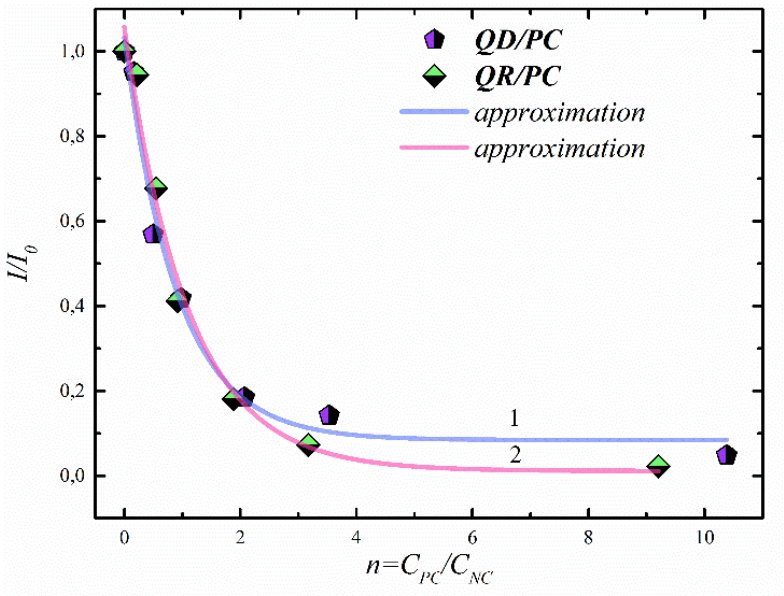

Fig. 5.7 Dependences of the relative intensity of luminescence of QD and QR on the relative concentration of PC in the mixture ($n = C_{PC} / C_{NC}$): (**1**) the experimental data of QD and the approximation of experimental data of QD with function y = 0.94 • exp (-1.1n) +0.08 and (**2**) the experimental data of QR and the approximation of experimental data of QR function y = 1.04 • exp (-0.98n).

The Figure 5.7 shows that the curves of quenching of luminescence of complexes QD/PC and QR/PC with increasing concentration of PC molecules in the mixture are similar in nature. The average number of molecules, coupled with one NC, obeys the Poisson distribution [70], and, therefore, the quenching curve for QD and QR were approximated by a function:

$$\frac{I}{I_0} = Ae^{-tn} + (1 - A), \qquad \textbf{5.2}$$

where I and I_0 are the intensity of donor luminescence in the presence and absence of acceptor molecules, respectively. The parameter A that determines the fraction of donors, which are able to bind to the complex of molecules ($0 \le A \le 1$) was $A_{QD} \approx A_{QR} \approx 1$. The parameter value of t was not dependent on the type of the nanocrystals, used in the experiments, and was ~ 1. This means that one phthalocyanine molecule quenches the luminescence in average one QD and one QR. Complete quenching of NC's in complex with PC's was also confirmed by the study of their luminescence kinetics. An analysis of experimental data indicates the statistical mechanism of quenching with the formation of

complexes associated with energy transfer. In the QD/PC and QR/PC complexes, the coupling of one acceptor molecule results in the complete quenching of the donor.

The energy transfer efficiency can be defined as the ratio of the luminescence quantum yield of sensitized acceptor φ_{DA} to the luminescence quantum yield of the acceptor φ_A, caused by direct photoexcitation of molecules (see Chap. 2, the Formula 2.10).

As it can be seen from Fig. 5.8(a), the dependence of the quantum yield of sensitized luminescence, associated in a complex with NC's molecules of the acceptor in monomeric form, on the relative concentration of the acceptor in the mixture, that was calculated in accordance with Formula 5.1.

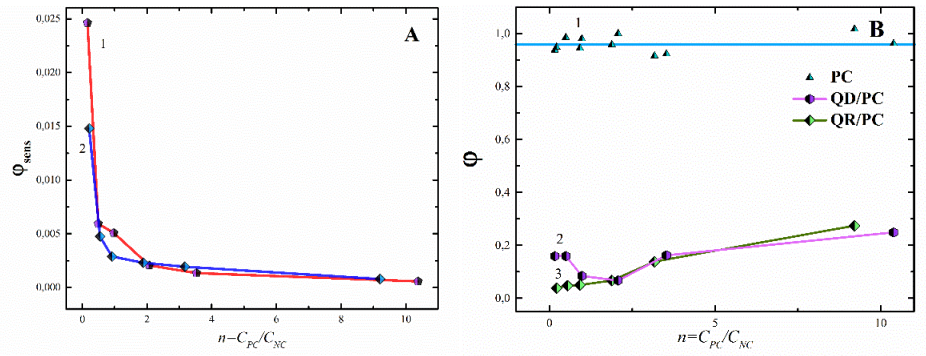

Fig. 5.8 (a) Dependences of the quantum yield of sensitized luminescence of PC on the relative concentrations of PC ($n = C_{PC}/C_{NC}$) in a mixture of: 1 – QD, 2 – QR; (b) dependence of the relative quantum yield of PC luminescence on relative concentration of PC in a mixture: 1 – PC molecules in free shape, 2, 3 – compound QD-PC and QR-PC, respectively.

Figure 5.8. (a) presents an increase of concentration of the PC acceptor molecules in a mixture of nanocrystals, leading to a sharp exponential drop of the quantum yield of sensitized luminescence of PC monomers in the case of QD/PC complexes as well as in the case of QR/PC. This might be due to the decrease in efficiency and decrease of the quantum yield of PC luminescence.

Figure 5.8 (b) shows the dependences of the relative quantum yield of luminescence of PC molecules. It is evident that the formation of QD/PC and QR/PC complexes leads to a sharp drop in the quantum yield of luminescence of PC molecules. At the molar concentration ratio more than 0.2:1, there is exponential decrease in the luminescence quantum yield of PC. That's probably can be attributed to the formation of

the aggregation of PC molecules in the complexes. The increase in the quantum yield of PC luminescence in a mixture of QR correlates with the dependence of the relative contents of PC aggregates in these samples. It should be noted that a sufficiently small content of aggregates (10%) in the QR/PC complexes with large concentrations of PCs in the mixture, could not explain such a strong luminescence quenching of PC in a mixture with QR and it indicates the presence of another efficient nonradiative deactivation channel of the excited PC state. A similar situation is observed in the complexes with QDs.

Figure 5.9 shows the values of efficiency of energy transfer, calculated by the formula 2.10 (see Chap. 2).

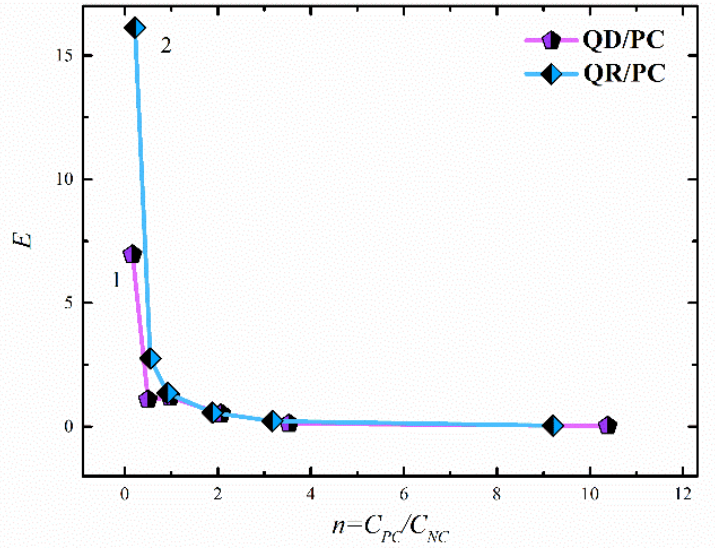

Fig. 5.9 Dependence of the efficiency of energy transfer (*E*) on the relative concentrations of PC $n = C_{PC}/CNC$ in QD-PC and QR-PC complexes: *1* – QD-PC; *2* – QR-PC.

Fig. 5.9 shows that with the increase of PC concentration in complexes with QD and QR, there is a dramatic decrease of the efficiency of energy transfer. Herewith, the values of the efficiency of energy transfer for donor-acceptor pairs QD-PC and QR-PC at low relative concentrations of phthalocyanine have the efficiency of energy transfer around 7% for QD/PC and 16% for QR/PC, despite previously identified formation of aggregates in complexes with NC's. One can note that the dependence of the efficiency of energy transfer in the QD/PC complexes on the total concentration of PC in the mixture correlates well with the dependence of relative content of PC aggregates in this system. At the same time, the comparison of the dependencies of relative content of PC

aggregates and FRET efficiency in QR/PC complexes clearly indicates that in the complexes of NC/PC, there is a new channel of deactivation of the excited state, which competes with intracomplex FRET and PC luminescence, and the efficiency of which increases with the increase of the average number of PC in the complexes.

5.3 Conclusions

The complexes of semiconductor CdSe/ZnS of quantum dots and quantum rods (coated cysteamine molecules) with organic molecules of sulfophthalocyanine were formed. The formation of the complexes occurred via electrostatic interaction of oppositely charged NC and PC. Analysis of the spectral data revealed the appearance of a band that corresponds to the aggregated form of PC molecules in the complex of NC/PC. We also calculated the percentage of PC aggregates in complexes with NC. In the case of the QR, at the first addition of PC, there is about 55% of aggregates, and, with the increasing concentration of PC in the complex, it decreases exponentially. The opposite situation is observed in QD/PC complexes. At the first addition, the percentage of PC aggregates was 10% and then it started to increase exponentially with increasing relative concentrations of PC. Analysis of the spectral-luminescent properties of NC/PC complexes showed that at relatively low concentrations of PC in the complex, there is an efficient energy transfer between the NC and PC. However, the increase of PC concentration leads to a sharp exponential drop in the efficiency of energy transfer. It was revealed that the increase in the total concentration of PC in the samples, in the case of a mixture with QR, leads to a decrease in the relative content of PC aggregates and to the drop in FRET efficiency in the complexes with QR. Such behavior of the system clearly indicates the formation of a new channel for nonradiative deactivation of the excited state of the system, which is not associated to the formation of nonluminescent aggregates and the efficiency of which has a distinct dependence on PC concentration.

Chapter 6. Water-soluble NC/PC complexes in DMSO

6.1 Features of formation water-soluble complexes NC/PC in DMSO

In the previous Chapter it was shown that the loss of charge of PC, when it is associated in complex with NC, leads to PC aggregation in complexes. Therefore, a study of formation conditions and properties of NC/PC complexes in dimethyl sulfoxide (DMSO), where tetrapyrrole molecules are usually less susceptible to aggregation, was carried out.

Unlike electrostatic binding of NC/PC in distilled water shown in the previous Chapter, in DMSO there is no dissociation of sulfogroup molecules of PC and protonation of cysteamine molecules on the surface of NC. Therefore, the formation of water-soluble complexes NC/PC in DMSO, is likely to occur as a result of hydrogen bond between nitrogen atoms of cysteamine amino group and sulfophthalocyanine sulfo group.

6.2 Optical properties of NC/PC complexes in DMSO

To form the complexes of NC and PC organic molecules by a hydrogen bond, QD and QR of core/shell type CdSe/ZnS, stabilized by hydrophilic molecules of cysteamine, were used. Concentration of nanocrystals in the solution of DMSO was for QDs (C_{QD} = 7x10^{-8} mol/L) and QRs (C_{QR} = 1.5x10^{-8} mol/L), respectively.

It should be noted that when adding NCs in DMSO, there was a decrease in the quantum yield of luminescence of QD and QR compared to the aqueous solutions, which lead to a change of Förster radius data for D-A pairs. Table 6.1 shows NC data in DMSO.

Table 6.1 Theoretical estimation of FRET parameters for systems NC/PC in DMSO

NC type	*J*, $M^{-1} cm^3$	Luminescence quantum yield, %	R_0,nm	*R*, nm	E_{th}
QD	5.56×10^{-12}	2	5.24	3.64	89 %
QR	6.314×10^{-12}	7	6.46	3.64	96%

Figure 6.1 shows the absorption spectra of QD, PC and mixed solutions of CdSe/ZnS QD/PC at different ratios of molar concentrations of the components in the mixture ($n = C_{PC}/C_{NC}$) in DMSO solution.

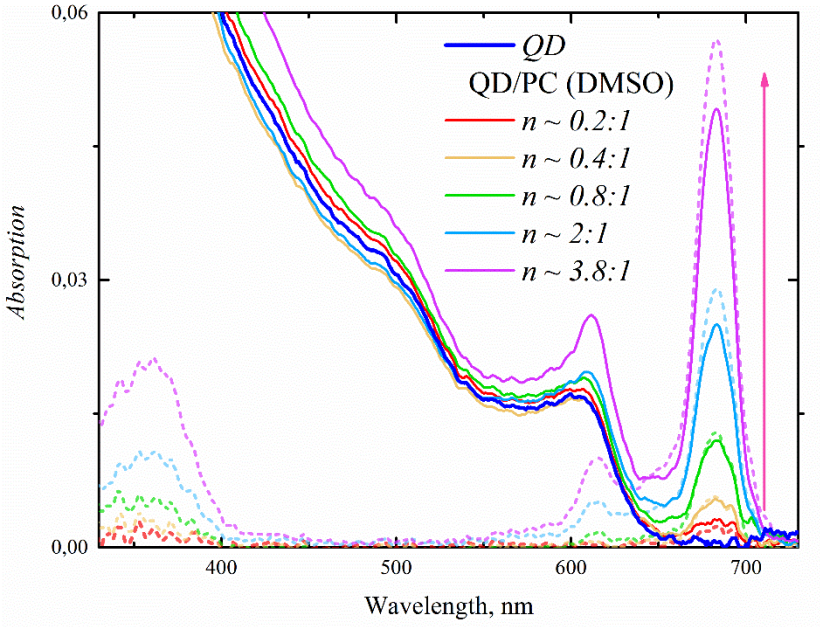

Fig. 6.1 Absorption spectra of solutions:QD, free PC and mixed solutions QD/PC with increasing the relative concentration of PC molecules in DMSO.

The study of mixed solutions of QD/PC at different ratios of molar concentrations of the components were carried out 60 minutes after preparation of the mixtures. From the analysis of the absorption spectra of mixed solutions of QD/PC, it is clear that the spectra represent the additive sum of the components of the PC and QD. One can note that based on the analysis of the absorption spectrum, it is impossible to conclude on the formation of complexes between QD and PC. It can be seen from Fig. 6.1 that with increasing of relative concentration of PC, in the PC absorption spectrum there is an increase in the intensity of the first band Q(I) of absorption. Comparing the absorption spectra of PC in DMSO to the spectra of the PC in distilled water (see Chap. 5, Fig. 5.2), one can see in the mixed solution QD/PC and PC in a free shape, the bathochromic shift of ~ 7 nm of Q – band is observed.

Further, the difference absorption spectra of PC of mixed solutions QD/PC were obtained from the experimental data (Fig. 6.2).

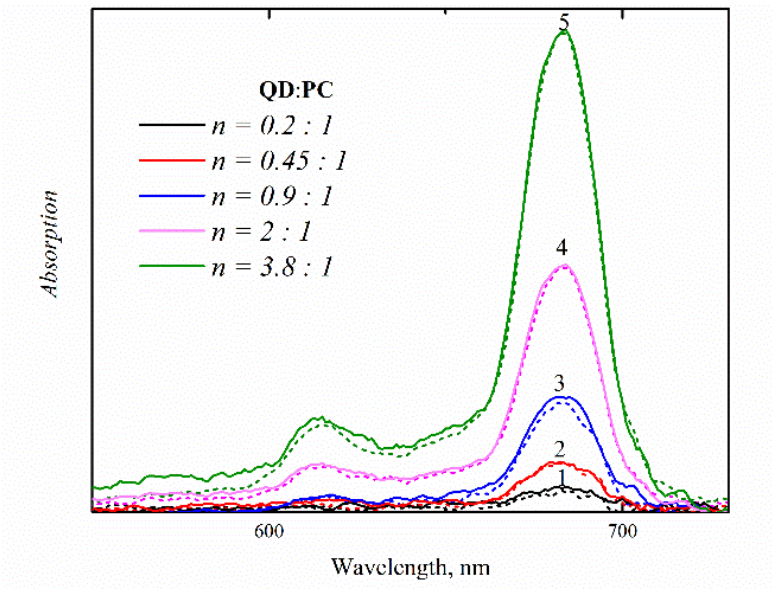

Fig. 6.2. Absorption spectra of PC: (*solid line*) difference absorption spectra of PC photosensitizer in mixed solutions QD/PC; (*dotted line*) sample of free PC with the concentration of photosensitizer molecules (*1*- ***0.2:1***, *2*- ***0.45:1***, *3*- ***0.9:1***, *4*- ***2:1***, *5*- ***3.8:1***)

The obtained difference absorption spectra of PC molecules are similar in nature to the absorption spectrum of PC in a molecular form. Here the analysis of the absorption spectra of PC in a mixture of QD/PC compared to free PC in DMSO showed no signs of aggregation of PC molecules that were observed with increasing concentration of PC in the case of NC/PC complexes in aqueous solutions at the wavelength of 640 nm (see Chap. 5, Fig. 5.3).

Figure 6.3 shows the luminescence spectra of CdSe/ZnS QD and mixed solutions QD/PC and PC molecules in DMSO at different ratios of molar concentration of PC and QD. The excitation of luminescence light was at a wavelength of 475 nm.

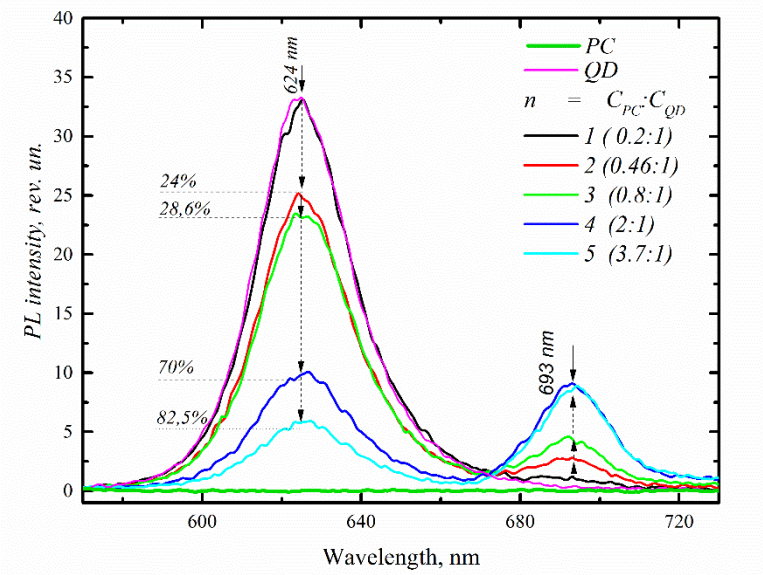

Fig. 6.3. Luminescence spectra of mixed solutions of QD/PC in DMSO and PC in a free shape (C_{PC}~2.8x10^{-7} mol/L) under light emission at λ=*475 nm*.

Fig. 6.3 shows that with an increase in the relative concentration of the acceptor molecules in the QD/PC complexes, the effective luminescence quenching of QD. Along with QD luminescence quenching, PC sensitized luminescence with a peak at ~ 693 nm is observed. The appearance of PC sensitized luminescence presents intracomplex photoexcitation energy transfer and, therefore, the formation of complexes between QD and PC.

Figure 6.4 shows the spectra of luminescence excitation of a mixture QD/PC and the absorption spectrum of QD. Recording of excitation luminescence spectra of the mixed solutions was performed at the wavelength of 700 nm. It should be noted that normalization was performed by a first band absorption amplitude Q(I) PCs, which corresponds to the normalization in the luminescence quantum yield and PC concentration and makes it easy to compare the efficiency of FRET at different relative concentrations (*n*) of PC in the sample s.

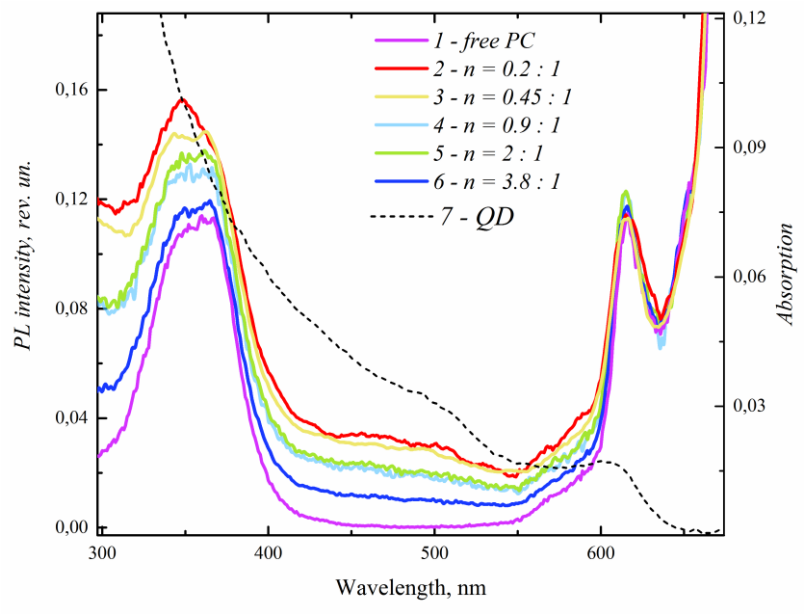

Fig. 6.4. Excitation luminescence spectra: 1 – PC free form, 2-6 excitation spectra of QD/PC in DMSO with increasing relative concentrations of PC. Recording of spectra was carried out at the wavelength of 700 nm. 7 - absorption spectrum of QD.

The comparison of the luminescence excitation spectra of the QD/PC complexes to the luminescence excitation spectra of free-shape PC and the absorption spectrum of QD, allows us to conclude that in complexes there is the energy transfer from QD to PC take place as evidenced by the contribution of the absorption spectrum of QD to the excitation spectrum of PC luminescence in the range of 400-600 nm. Herewith, it is clear that the contribution of QD absorption to the excitation spectrum of PC luminescence decreases with increasing concentration of PC in the mixture. It should be noted that in DMSO the formation of complexes is most likely due to the formation of hydrogen bonds between the nitrogen of the cysteamine amino group and sulfo phthalocyanine. Therefore, in contrast to aqueous solutions, the observed decrease of FRET efficiency with increasing *n* may be due to increase in the effectiveness of nonradiative channels of deactivation of the excited state, competing with FRET, so that not all PC is linked to the complex with QD.

Figure 6.5 shows the dependence of relative intensity of QD ratio on the molar concentrations of the components in the mixture of QD/PC.

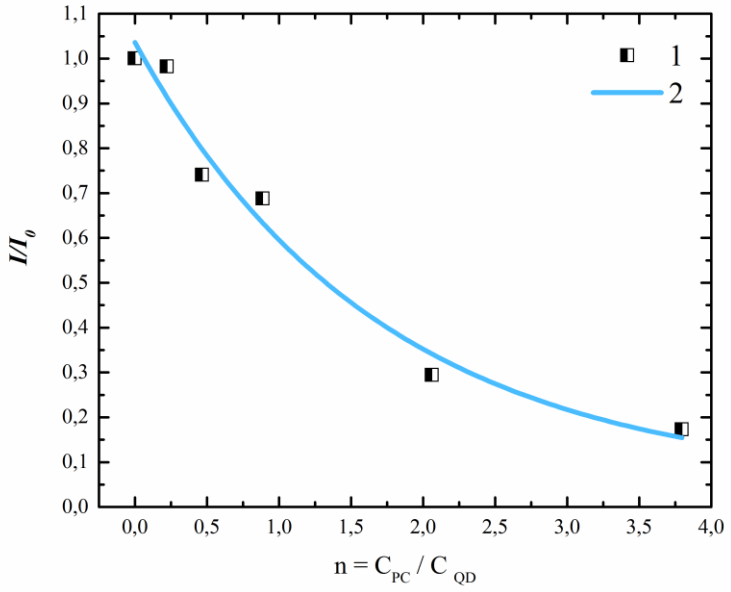

Fig. 6.5. Dependence of relative luminescence intensity (I/I0) of QD on the ratio of the concentrations C_{PC}/C_{QD} in the QD/PC complexes: 1 – experimental data; 2 – approximation of the function *y = 0,98 exp (- 0,59 n) +0,05*.

From Fig. 6.5 one can conclude that the curve quenching of luminescence of QD with increasing relative concentration of PC in a mixture with QD in DMSO has an exponential form in the same way as in the case of NC/PC complexes in aqueous solution when implementing electrostatic binding approach (see Chap. 5, Fig. 5.7). It is known that the quenching curve can provide information about the average number of NCs, which are quenching one PC molecule. The dependence of QD luminescence intensity was approximated by the function y = *0,98·exp(-0,59·n) +0,05*. A factor of 0.59 means that one molecule of PC quenches 1 QD by the amount of 60 %. Since this value is significantly lower than the theoretical efficiency of FRET for this D-A pair (see. Table 5.1), it could be assumed that this factor reflects relative number of PC molecules, that are to coupled in the complex with QD's.

Figure 6.6 shows the luminescence spectra of PC molecules in free form and in complex with QD for different concentrations of PC in the mixture when excited by light at a wavelength of 665 nm.

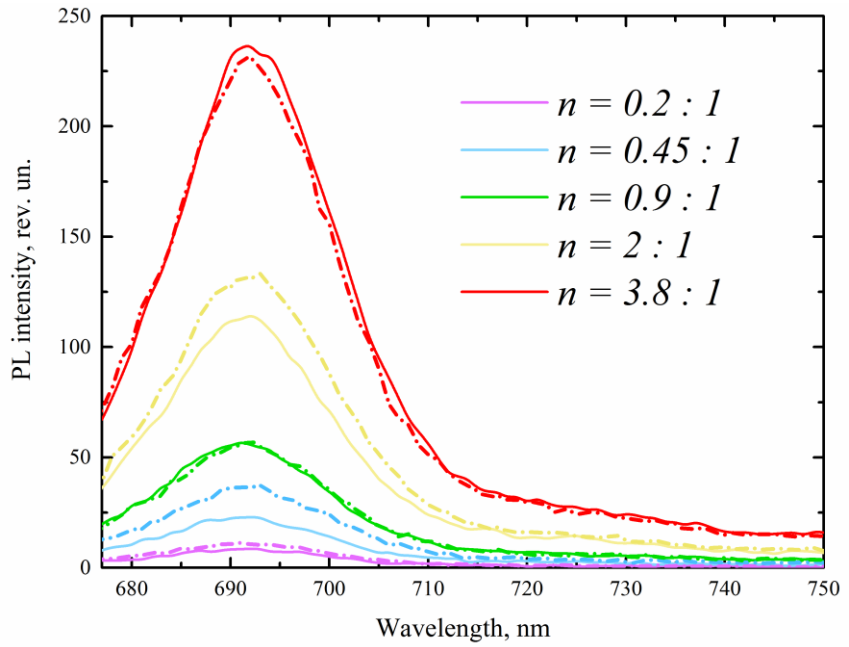

Fig. 6.6 Luminescence spectra of the mixture of QD and PC and free PC in DMSO at different ratios of molar concentrations of the components in the mixture under light emission at 665 nm.

It Fig. 6.6 reveals that the luminescence intensity of PC in the mixture with QD's practically corresponds to the intensity of luminescence of free PC in solution. This indicates that in the mixture with QD's, the luminescence quantum yield of PC corresponds to the quantum yield of luminescence of free PC in DMSO. It should be noted that the preservation of the luminescence quantum yield of PC in the complexes with QD's allows one to expect the preservation of its photosensitizing properties, i.e. the quantum yield of generation of singlet oxygen.

Also in DMSO, the interaction of QR with PC was investigated, but for a fixed ratio of the molar concentrations of the components in the mixture. An analysis of photophysical properties of QD/PC complexes showed that not all PC molecules in the mixture were coupled with QD complex. One reason for the incomplete binding of the components in the complex could be the short time after the preparation of mixed solutions. Therefore, to study PC interaction with QR in DMSO, the mixtures were maintained under normal conditions in the dark for 12 hours. It should also be noted that, for QR, our study was performed only for a fixed ratio of PC/QR (n = 19).

Figure 6.7 shows the absorption spectra of CdSe/ZnS QR, PC and a mixed solution of QR/PC in DMSO at a ratio of molar concentration of mixture components $n = 19$.

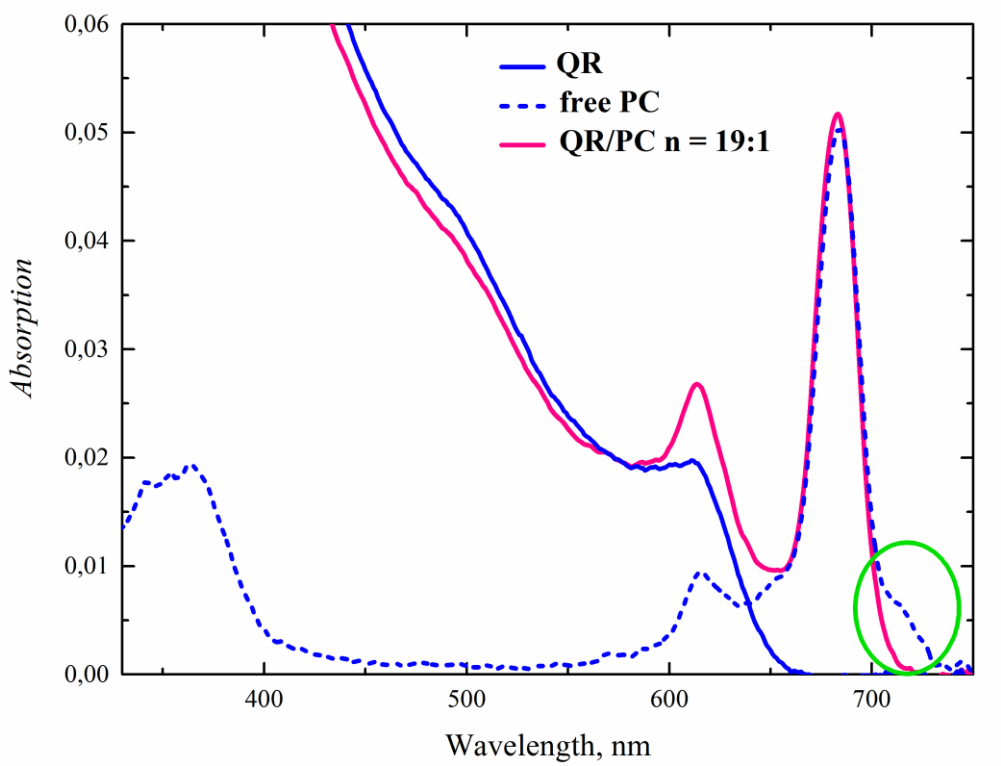

Fig. 6.7 Absorption spectra: QR, free PC and a mixed solution of QR/PC at a ratio of molar concentrations of the components of QR: PC (*n*=19) in DMSO

Fig. 6.7 shows that the broadening of the red edge of the Q-band at 720 nm of free PC at a concentration of PC ~10^{-7} mol/L. According to the literature review, it is connected to the formation of J-aggregates PC [71]. Herewith, the analysis of the absorption spectra of PC in a mixture of QR showed that unlike free PC in a mixture with QR, there are no signs of phthalocyanine aggregation, i.e. the presence in the solution of QR inhibits the aggregation of PC. Shown in Fig. 6.9, the luminescence spectra of QR in the absence of PC molecules in the mixture and QR in complex with PC were recorded with excitation by light at a wavelength of 475 nm.

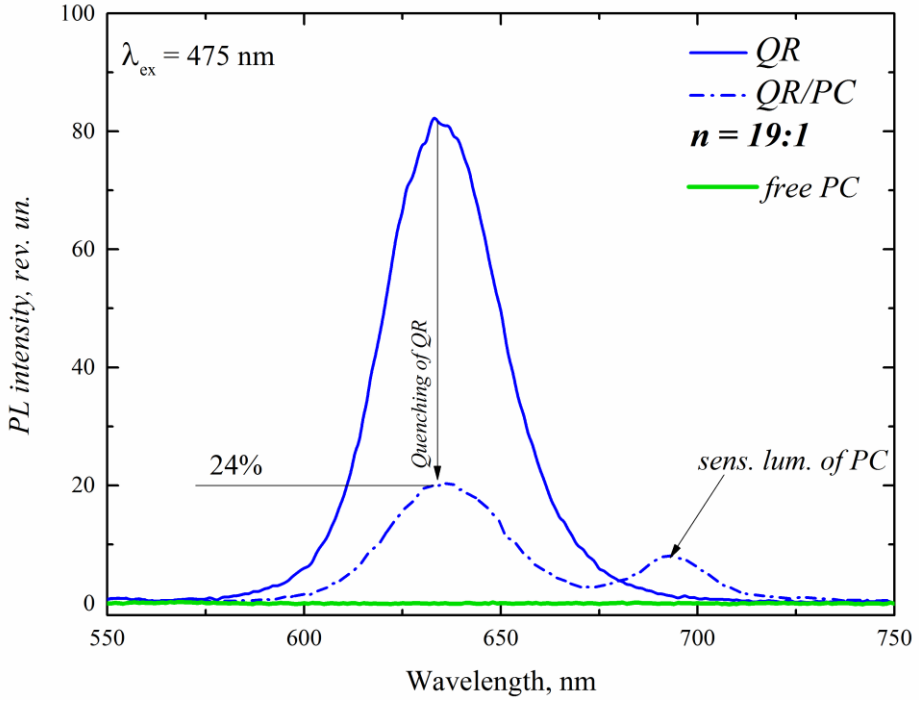

Fig. 6.9 Luminescence spectra of the mixed solution of QR/PC, PC in a free form ($C_{PC} \sim 2.8 \cdot 10^{-7}$ mol/L) in DMSO (*n = 19*) when excited by light at a wavelength of 475 nm.

From Fig. 6.9 one can that when we add PC molecules to a solution of QR, there is some luminescence quenching by the amount about 76 %. Similarly, as in the case of of QR/PC complexes, the appearance of sensitized luminescence of PC at 683 nm is observed. The spectrum of luminescence of free PC, shown in Fig. 5.9, also presents that the luminescence of PC in a mixture of QR is due to the energy transfer of QR.

Figure 6.10 presents the spectra of luminescence excitation for a mixture QR/PC (*n=19:1*) and PC in DMSO under light emissiona at the wavelength of 700 nm, and in comparison, we also include the absorption spectrum of QR.

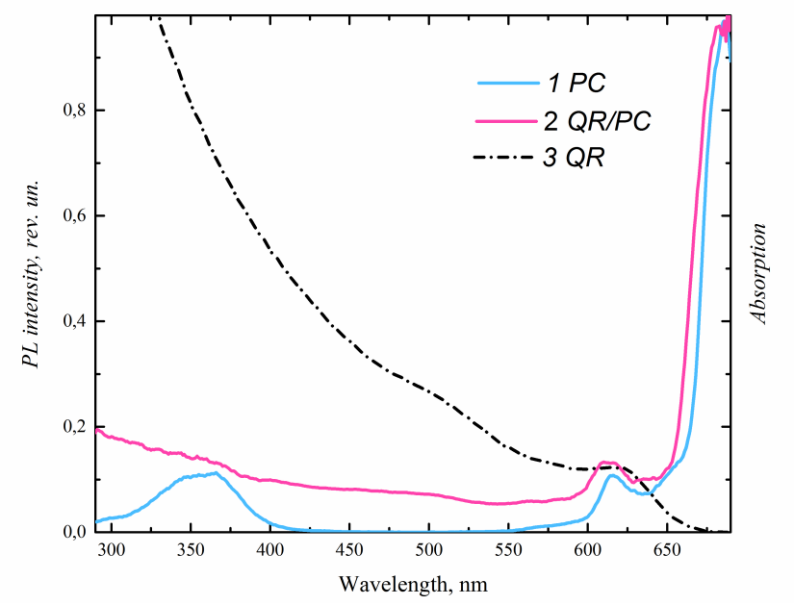

Fig. 6.10 Excitation spectra of luminescence of: 1 – PC; 2 –QR/PC complexes in DMSO; 3 – the absorption spectrum of QR. Recording of luminescence was carried out at the wavelength of 700 nm.

Excitation spectra of luminescence of QR/PC and free PC were normalized by the first absorption band of PC. As it evident from Fig. 6.10, in the excitation spectrum of PC luminescence in mixture with QR, the contribution to the absorption spectrum of QR is clearly visible, indicating the energy transfer from QR to PC.

6.3 Intracomplex energy transfer efficiency of NC/PC in DMSO

Figure 6.10 shows the dependence of energy transfer efficiency in the QD/PC complexes on the ratio of the molar concentrations of the components in the mixture using the formula 2.10 (see Chap.2). From the figure shows that with increasing of PC concentration in the complexes with QD there is an exponential decrease in the efficiency of energy transfer. It is shown in Fig. 6.10 that the efficiency of energy transfer with the first additive is about 0.42 (~42%).

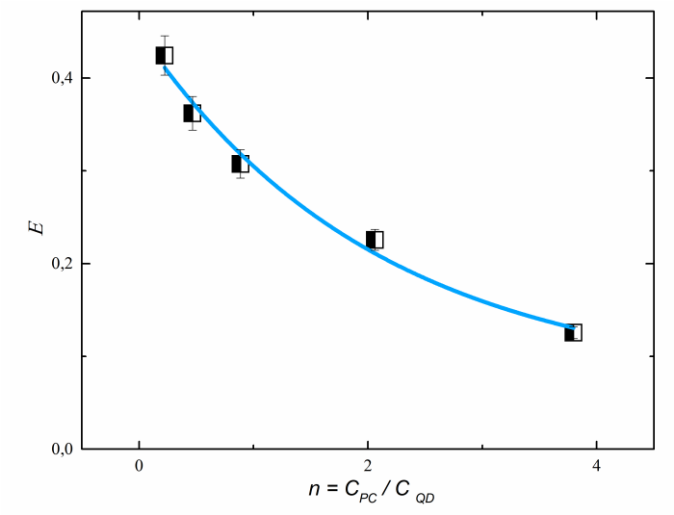

Fig. 6.10. Dependence of the energy transfer efficiency (*E*) on the relative concentrations of PC $n = C_{PC}/C_{QD}$ in the QD/PC complexes.

The energy transfer efficiency of QR/PC was calculated at *n = 19*, the value of which amounted to 18%. Evaluation of the efficiency of FRET, using the Formula 2.10 (see Chap. 2), in this case could only give a lower limit of this value because the relative amount of PC, associated in complex, is unknown and the evaluation falls under the assumption that all PC molecules is coupled in complex with QR's.

5.4 Conclusions

From the analysis of spectral-luminescent properties of CdSe/ZnS QD, QR and PC, it follows that in the solution of DMSO observed the formation of QD/PC and QR/PC complexes presumably by hydrogen bonds. In this systems with increasing the relative concentration of acceptor molecules there is an effective energy transfer by FRET mechanism. It was found, in the systems of NC's/PC in DMSO on the absorption spectra there are no cause of aggregation, unlike of NC's/PC complexes in aqueous solution via electrostatic interaction. The preservation of the quantum yield of PC luminescence in the complexes with QD and QR leads to the conclusion that the observed reduction in the efficiency of energy transfer in the QD/PC complexes in DMSO is due to the presence of free PC in the samples or the aggregation of QD.

SUMMARY

This thesis is devoted to the study of photophysical properties and spectral-luminescent properties of complexes of semiconductor CdSe/ZnS quantum dots and quantum rods in the interaction with tetrapyrrole molecule of Al(OH)-sulfophthalocyanine. The following results were obtained:

— The formation of the complexes of cationic CdSe/ZnS quantum dots and quantum rods, coated by cysteamine molecules, with organic molecules of sulfophthalocyanine in aqueous solution by electrostatic interaction.

— It was established that with the formation of complexes of quantum dot/sulfophthalocyanine and quantum rods/sulfophthalocyanine in aqueous solutions the aggregation of PC occurs.

— It was established that the shape and size of NC have a significant influence on the concentration of PC aggregates in the complexes with NC in aqueous solutions.

— It was revealed that in an aqueous solutions in NC/PC complexes there is the formation of a new nonradiative channel of deactivation of the excited state of NCs and PCs, which is not caused the formation of nonluminescent PC aggregates and competes with the FRET and quantum yield of PC luminescence. It is shown that the efficiency of this process increases with the increase of PC concentration in the samples.

— Water-soluble complexes CdSe/ZnS quantum dots and quantum rods with molecules of sulfophthalocyanine, formed by hydrogen bond between the amino nitrogen atoms and sulfo group of sulfophthalocyanine, in dimethyl sulfoxide were obtained.

— It was shown that unlike of NC/PC complexes in an aqueous solution, the formation of NC/PC complexes in DMSO causes no aggregation of PC molecules.

— In the NC/PC complexes in dimethyl sulfoxide there is effective photoexcitation energy transfer from donor to acceptor molecules.

Thus, it was demonstrated for the first time that in the complexes of semiconductor nanocrystals, the inhibition of aggregation of the photosensitizer allows to realize an efficient energy transfer of photoexcitation and preserve photophysical properties of the photosensitizer.

The results, obtained in the Master's thesis, are relevant today and clearly demonstrate the ability to develop a new generation of photosensitizers for effective

diagnosis and treatment of oncological diseases, based on colloidal quantum semiconductor nanocrystals.

The results of this work, presented in Chapter 4,5, are published in the following paper:

D. R. Dadadzhanov, I. V. Martynenko, A. O. Orlova, V. G. Maslov, A. V. Fedorov, and A. V. Baranov The Formation of Molecular Aggregates of Sulfophthalocyanine in Complexes with Semiconductor Nanocrystals // Optics and Spectroscopy, 2015, Vol. 119, No. 5, pp. 738–743 3

D.R. Dadadzhanov, I.V. Martinenko Исследование условий агрегации молекул сульфофталоцианина в комплексах с CdSe/ZnS квантовыми точками и квантовыми стержням //Сборник тезисов докладов конгресса молодых учёных, Санкт-Петербург: Университет ИТМО, 2015

D. R. Dadadzhanov, I. V. Martynenko, A. O. Orlova, V. G. Maslov, A. V. Fedorov, and A. V. Baranov Образование молекулярных агрегатов сульфофталоцианина в комплексах с полупроводниковыми нанокристаллами // Оптика и спектроскопия - 2015. - Т. 119. - № 5. - С. 712-717", 2015

D. R. Dadadzhanov, I. V. Martynenko, A. O. Orlova, V. G. Maslov, A. V. Fedorov, and A. V. Baranov Aggregation of Sulfophthalocyanine in Complexes with CdSe/ZnS Quantum Dots and Quantum Rods// PCNSPA Conference 2016 - Photonic Colloidal Nanostructures: Synthesis, Properties, and Applications//Book of Abstract, p 77. ,2015

References

1. Efros, A.L., D.J. Lockwood, and L. Tsybeskov, *Semiconductor Nanocrystals: From Basic Principles to Applications*. 2003: Springer.
2. Michalet, X., et al., *Quantum Dots for Live Cells, in Vivo Imaging, and Diagnostics.* Science, 2005. 307: p. 538.
3. Dougherty, T.J., et al., *Photodynamic Therapy.* Journal of the National Cancer Institute, 1998. 90(12): p. 889-905.
4. Alivisatos, A.P., *Semiconductor clusters, nanocrystals, and quantum dots.* Science, 1996. 271(5251): p. 933.
5. Ekimov, A.I., A.L. Efros, and A.A. Onushchenko, *Quantum size effect in semiconductor microcrystals.* Solid State Communications, 1985. 56(11): p. 921-924.
6. Gaponenko, S., *Optical Properties of Semiconductor Nanocrystals*. 1998.
7. Rafailov, E.U., M.A. Cataluna, and E.A. Avrutin, *Ultrafast Lasers Based on Quantum Dot Structures: Physics and Devices*. 2011: John Wiley & Sons.
8. Ozin, G.A., A.C. Arsenault, and L. Cademartiri, *Nanochemistry: a chemical approach to nanomaterials*. 2009: Royal Society of Chemistry.
9. Hoeppener, S., et al., *Metal Nanoparticles, Nanowires, and Contact Electrodes Self-Assembled on Patterned Monolayer Templates—A Bottom-up Chemical Approach.* Advanced Materials, 2002. 14(15): p. 1036-1041.
10. Chan, H.-K. and P.C.L. Kwok, *Production methods for nanodrug particles using the bottom-up approach.* Advanced drug delivery reviews, 2011. 63(6): p. 406-416.
11. Thakkar, K.N., S.S. Mhatre, and R.Y. Parikh, *Biological synthesis of metallic nanoparticles.* Nanomedicine: Nanotechnology, Biology and Medicine, 2010. 6(2): p. 257-262.
12. *Quantum dots light up under strain*. Available from: http://phys.org/news/2015-09-quantum-dots-strain.html
13. Murray, C., D.J. Norris, and M.G. Bawendi, *Synthesis and characterization of nearly monodisperse CdE (E= sulfur, selenium, tellurium) semiconductor nanocrystallites.* Journal of the American Chemical Society, 1993. 115(19): p. 8706-8715.
14. Dabbousi, B.O., et al., *(CdSe)ZnS Core−Shell Quantum Dots: Synthesis and Characterization of a Size Series of Highly Luminescent Nanocrystallites.* The Journal of Physical Chemistry B, 1997. 101(46): p. 9463-9475.
15. *Optical Properties of ZnO Nanorods and CdSe/ZnS Quantum Dots;CuO Nanostructures*. 2007: National Taiwan University Department of Physics .

16. http://www.nanosysinc.com/what-we-do/quantum-dots/. *Quantum dots are used in commercial Quantum Dot Enhancement Film (QDEFTM)*.
17. Salata, O.V., *Applications of nanoparticles in biology and medicine.* Journal of Nanobiotechnology, 2004. 2(1): p. 1-6.
18. Mah, C., et al., *Improved method of recombinant AAV2 delivery for systemic targeted gene therapy.* Mol Ther, 2002. 6(1): p. 106-12.
19. Parak, W.J., et al., *Biological applications of colloidal nanocrystals.* Nanotechnology, 2003. 14.
20. Nam, J.M., C.S. Thaxton, and C.A. Mirkin, *Nanoparticle-based bio-bar codes for the ultrasensitive detection of proteins.* Science, 2003. 301(5641): p. 1884-6.
21. Juzenas, P., et al., *Quantum dots and nanoparticles for photodynamic and radiation therapies of cancer.* Advanced drug delivery reviews, 2008. 60(15): p. 1600-1614.
22. Salata, O.V., *Applications of nanoparticles in biology and medicine.* Journal of Nanobiotechnology, 2004. 2: p. 3-3.
23. Juzeniene, A., *Chlorin e6-based photosensitizers for photodynamic therapy and photodiagnosis.* Photodiagnosis and Photodynamic Therapy. 6(2): p. 94-96.
24. Bonnett, R., *Photosensitizers of the porphyrin and phthalocyanine series for photodynamic therapy.* Chemical Society Reviews, 1995. 24(1): p. 19-33.
25. Gaspar, L.E. and M. Ding, *A review of intensity-modulated radiation therapy*. Current oncology reports, 2008. 10(4): p. 294-299.
26. Guillem, J.G., et al., *ASCO/SSO review of current role of risk-reducing surgery in common hereditary cancer syndromes.* J Clin Oncol, 2006. 24(28): p. 4642-60.
27. Paszko, E., et al., *Nanodrug applications in photodynamic therapy.* Photodiagnosis and Photodynamic Therapy. 8(1): p. 14-29.
28. Tegos, G., et al., *Concepts and principles of photodynamic therapy as an alternative antifungal discovery platform.* Frontiers in Microbiology, 2012. 3.
29. Osovsky, R., et al., *Electrostatic and covalent interactions in CdTe nanocrystalline assemblies.* The Journal of Physical Chemistry B, 2005. 109(43): p. 20244-20250.
30. Knoblauch, C., M. Griep, and C. Friedrich, *Recent Advances in the Field of Bionanotechnology: An Insight into Optoelectric Bacteriorhodopsin, Quantum Dots, and Noble Metal Nanoclusters.* Sensors, 2014. 14(10).

31. Moeno, S. and T. Nyokong, *The photophysical studies of a mixture of CdTe quantum dots and negatively charged zinc phthalocyanines.* Polyhedron, 2008. 27(8): p. 1953-1958.
32. Orlova, A.O., et al., *Investigation of Complexes of CdTe Quantum Dots with the AlOH-Sulphophthalocyanine Molecules in Aqueous Media.* The Journal of Physical Chemistry C, 2013. 117(44): p. 23425-23431.
33. Shi, L., B. Hernandez, and M. Selke, *Singlet Oxygen Generation from Water-Soluble Quantum Dot−Organic Dye Nanocomposites.* Journal of the American Chemical Society, 2006. 128(19): p. 6278-6279.
34. Britton, J., E. Antunes, and T. Nyokong, *Fluorescence quenching and energy transfer in conjugates of quantum dots with zinc and indium tetraamino phthalocyanines.* Journal of Photochemistry and Photobiology A: Chemistry, 2010. 210(1): p. 1-7.
35. Clegg, R.M., *Fluorescence resonance energy transfer*. Current opinion in biotechnology, 1995. 6(1): p. 103-110.
36. Ермолаев В.Л., Б.Е.Н., Свешникова Е.Б., Шахвердов Т.А., *Безызлучательный перенос энергии электронного возбуждения.* «Наука»: p. 311.
37. Gilmore, A.M., *Luminescence: The Instrumental Key to the Future of Nanotechnology*. 2013: Pan Stanford.
38. Held, P., *An Introduction to Fluorescence Resonance Energy Transfer Technology and Its Application in Bioscience.* Bio Tek, 2005.
39. Lakowicz, J., *Principles of Fluorescence Spectroscopy*. 2007.
40. Artemyev, M., E. Ustinovich, and I. Nabiev, *Efficiency of Energy Transfer from Organic Dye Molecules to CdSe−ZnS Nanocrystals: Nanorods versus Nanodots.* Journal of the American Chemical Society, 2009. 131(23): p. 8061-8065.
41. Sadhu, S. and A. Patra, *Donor-acceptor systems: energy transfer from CdS quantum dots/rods to Nile Red dye.* Chemphyschem, 2008. 9(14): p. 2052-8.
42. Rebentrost, P., M. Stopa, and A. Aspuru-Guzik, *Forster coupling in nanoparticle excitonic circuits.* Nano letters, 2010. 10(8): p. 2849-2856.
43. Blanton, S.A., et al., *Dielectric Dispersion Measurements of CdSe Nanocrystal Colloids: Observation of a Permanent Dipole Moment.* Physical Review Letters, 1997. 79(5): p. 865-868.
44. Hu, J., et al., *Linearly polarized emission from colloidal semiconductor quantum rods.* Science, 2001. 292(5524): p. 2060-2063.

45. Schmelz, O., et al., *Supramolecular complexes from CdSe nanocrystals and organic fluorophors.* Langmuir, 2001. 17(9): p. 2861-2865.
46. Boulesbaa, A., et al., *Competition between Energy and Electron Transfer from CdSe QDs to Adsorbed Rhodamine B.* The Journal of Physical Chemistry C, 2010. 114(2): p. 962-969.
47. Algar, W.R., et al., *Quantum dots as platforms for charge transfer-based biosensing: challenges and opportunities.* Journal of Materials Chemistry B, 2014. 2(45): p. 7816-7827.
48. Freeman, R. and I. Willner, *Optical molecular sensing with semiconductor quantum dots (QDs).* Chem Soc Rev, 2012. 41(10): p. 4067-85.
49. Camp, P.J., et al., *Aggregation of Copper(II) Tetrasulfonated Phthalocyanine in Aqueous Salt Solutions.* The Journal of Physical Chemistry A, 2002. 106(44): p. 10725-10732.
50. Palewska, K., et al., *Effect of electric permittivity of the solvent on aggregation process of the water-soluble sulfonated metal phthalocyanines.* Journal of Photochemistry and Photobiology A: Chemistry, 2011. 223(2–3): p. 149-156.
51. Palewska, K., J. Sworakowski, and J. Lipiński, *Molecular aggregation in soluble phthalocyanines – Chemical interactions vs. π-stacking.* Optical Materials, 2012. 34(10): p. 1717-1724.
52. Petrasek, Z. and D. Phillips, *A time-resolved study of concentration quenching of disulfonated aluminium phthalocyanine fluorescence.* Photochem Photobiol Sci, 2003. 2(3): p. 236-44.
53. Maya, E.M., et al., *Synthesis, aggregation behavior and nonlinear absorption properties of lead phthalocyanines substituted with siloxane chains.* Journal of Materials Chemistry, 2003. 13(7): p. 1603-1613.
54. Nevin, W.A., et al., *Electrochemistry and spectroelectrochemistry of mononuclear and binuclear cobalt phthalocyanines.* Inorganic Chemistry, 1987. 26(4): p. 570-577.
55. Monahan, A.R., J.A. Brado, and A.F. DeLuca, *Dimerization of a copper (II)-phthalocyanine dye in carbon tetrachloride and benzene.* The Journal of Physical Chemistry, 1972. 76(3): p. 446-449.
56. Dougherty, G., et al., *Electron spin resonance spectroscopic and spectrophotometric investigation of the binding of tetracationic porphyrins and porphyrazines with calf thymus DNA. Unequivocal evidence for intercalation.* Journal

of the Chemical Society, Faraday Transactions 2: Molecular and Chemical Physics, 1985. 81(12): p. 1739-1759.

57. Martynenko, I.V., et al., *Energy transfer in complexes of water-soluble quantum dots and chlorin e6 molecules in different environments.* Beilstein J Nanotechnol, 2013. 4: p. 895-902.

58. Kuznetsova, N.A., et al., *Sulfonated phthalocyanines: aggregation and singlet oxygen quantum yield in aqueous solutions.* Journal of Porphyrins and Phthalocyanines, 2003. 07(03): p. 147-154.

59. Artemyev, M., B. Möller, and U. Woggon, *Unidirectional Alignment of CdSe Nanorods.* Nano Letters, 2003. 3(4): p. 509-512.

60. APOLIKHIN, et al., *Adjuvant photodynamic therapy (PDT) with photosensitizer photosens for superficial bladder cancer. Experimental investigations to treat prostate cancer by PDT with photosens*. Vol. 8. 2007, Belligham, ETATS-UNIS: Society of Photo-Optical Instrumentation Engineers.

61. Kubin, R.F. and A.N. Fletcher, *Fluorescence quantum yields of some rhodamine dyes.* Journal of Luminescence, 1982. 27(4): p. 455-462.

62. Suresh, S. and C. Arunseshan, *Dielectric Properties of Cadmium Selenide (CdSe) Nanoparticles synthesized by solvothermal method.* Applied Nanoscience, 2014. 4(2): p. 179-184.

63. Navarro, D.A.G., et al., *Natural Organic Matter-Mediated Phase Transfer of Quantum Dots in the Aquatic Environment.* Environmental Science & Technology, 2009. 43(3): p. 677-682.

64. von Holt, B., et al., *Ligand exchange of CdSe nanocrystals probed by optical spectroscopy in the visible and mid-IR.* Journal of Materials Chemistry, 2008. 18(23): p. 2728-2732.

65. Callan, J. and F.M. Raymo, *Quantum Dot Sensors: Technology and Commercial Applications*. 2013: Pan Stanford.

66. Ananthakumar, S., J. Ramkumar, and S. Moorthy Babu, *Synthesis and Efficient Phase Transfer of CdSe Nanoparticles for Hybrid Solar Cell Applications.* Conference Papers in Energy, 2013. 2013: p. 3.

67. Zhang, Y. and A. Clapp, *Overview of Stabilizing Ligands for Biocompatible Quantum Dot Nanocrystals.* Sensors (Basel, Switzerland), 2011. 11(12): p. 11036-11055.

68. Jeong, S., et al., *Effect of the thiol-thiolate equilibrium on the photophysical properties of aqueous CdSe/ZnS nanocrystal quantum dots.* Journal of the American Chemical Society, 2005. 127(29): p. 10126-10127.
69. Wuister, S.F., C. de Mello Donega, and A. Meijerink, *Influence of thiol capping on the exciton luminescence and decay kinetics of CdTe and CdSe quantum dots.* The Journal of Physical Chemistry B, 2004. 108(45): p. 17393-17397.
70. Dworak, L., et al., *Acceptor Concentration Dependence of Förster Resonance Energy Transfer Dynamics in Dye–Quantum Dot Complexes.* The Journal of Physical Chemistry C, 2014. 118(8): p. 4396-4402.
71. Egorov, V.V. and M.V. Alfimov, *Theory of the J-band: from the Frenkel exciton to charge transfer.* Physics-Uspekhi, 2007. 50(10): p. 985-1029.